Semester project

FEM Simulations of resonator with passivation for measurements in liquid environment

Grégoire Albrand
Mechanical Engineering Faculty

Supervised by
Professor Guillermo Villanueva
Florian Hartmann

January 23, 2023

Contents

1 Introduction

This semester project, conducted in the Advanced NEMS laboratory, aims at studying and improving the behaviour of SH0 resonators. While previous semester projects on this subject [1] [2] [3] focused on their behaviour in air, and the optimization of the inactive region of the resonator, this work mainly focuses on the behaviour in water, and is supposed to improve the parameters of the active region (see figure 1). Indeed, the device is intended to work within a cell, playing the role of a cell tracker. The best way to simulate this cellular environment is therefore to proceed to simulations into water, and not in air anymore.

The device studied here presents however some differences with the one mentioned in previous semester projects. Indeed, first, the cut tested is 36° YX (and not 170°) in order to observe more important SH0 modes. Moreover, the device being constituted of electrodes normally exposed to the environment, we need to make some modifications in our case. Indeed, contact with water could generate short circuits that we wish to absolutely avoid. That's why a dielectric layer is added on the whole surface of the resonator.

It is also interesting to notice that, even if the quality of a resonator is mainly determined by 2 parameters, the quality factor and the coupling, only this latter will be analyzed here. Indeed, the quality factor depends majorly on the damping and thus on the losses. However, as the device is analyzed in an aqueous environment, losses are significant and depend on the damping defined manually in the COMSOL model. Quality factors obtained are therefore biased and non-representative of the real behaviour of the device. Moreover, this parameter wasn't meant to be optimized in this work.

In the following paragraphs, all useful quantities, as well as the devices analyzed, will be presented.

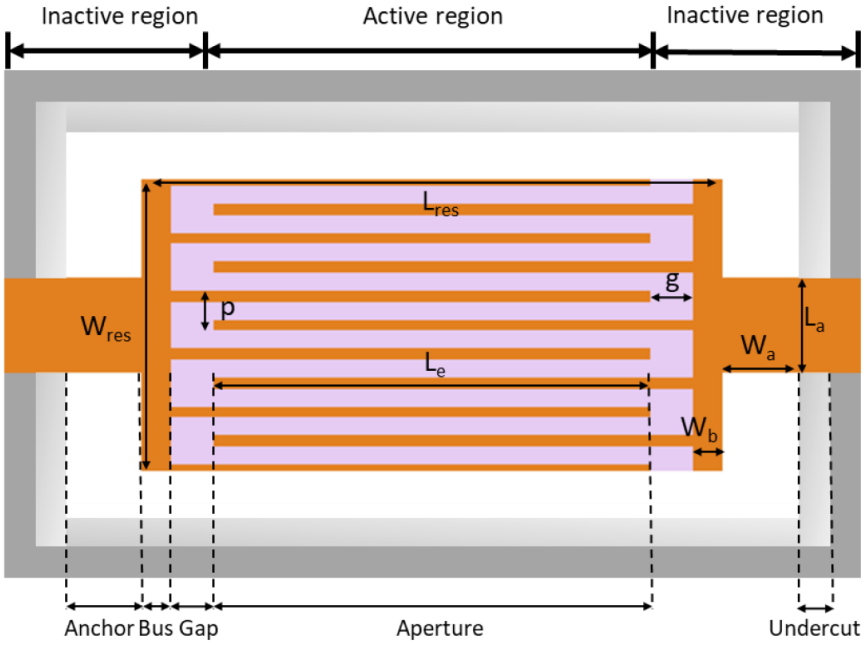

Figure 1: Presentation of a Lamb wave resonator [4]

1.1 Performance indicator

As explained above, the performance indicator used to evaluate the quality of the device will be the coupling coefficient. However, 3 different factors are commonly used : the piezoelectric coupling K^2, the electromechanical coupling factor k_t^2 (itself defined differently from one paper to another) and the effective coupling coefficient k_{eff}^2. Here, we will focus on the last one, defined by the following equation :

$$k_{eff}^2 = \frac{f_p^2 - f_s^2}{f_p^2} \tag{1}$$

Where f_p and f_s are respectively the anti-resonance and resonant frequencies. These different coupling factors are very close when the device presents a low coupling. Nevertheless, as shown by figure 2, this difference cannot be neglected anymore when the coupling increases.

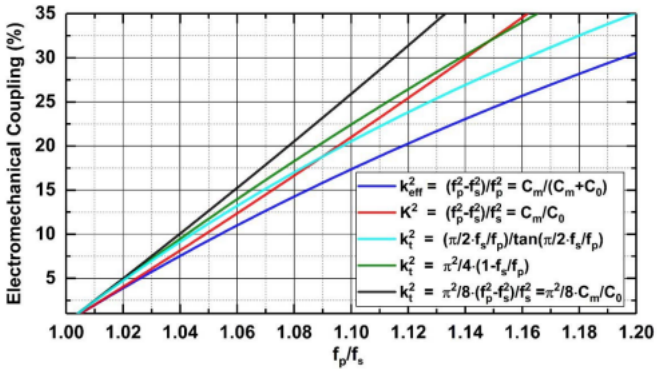

Figure 2: Comparison of the different coupling factors [5]

Figure 2 also shows one of the reasons behind the choice of k_{eff}^2 as the coupling coefficient of this study. Indeed, it is the more pessimistic estimation of the coupling. Therefore, using this value, the performance of the resonator won't be overestimated.

1.2 Models analyzed

3 COMSOL models were used during this project, all representing the same device, but with different configurations. The first and simplest one, is a 2D unit cell model (with the 3^{rd} component in the direction of the aperture) , consisting of the piezoelectric in $LiNbO3$, above which there are 2 electrodes, one connected with the signal, whereas the other is grounded. Finally, a layer of dielectric covers the electrodes and the piezoelectric. This model is the simplest one because it represents only one cell with Floquet periodicity boundary conditions applied on both sides. It is therefore equivalent to an infinite device barely impacted by perturbations (see figure 3).

The second device is still 2-dimensional but without periodic conditions. Indeed, all pairs of electrodes are represented, as well as the reflectors on the edges (see figure 4). This model can therefore be seen as the representation of the active region presented in figure 1. Finally, the third and last model is a 3D unit cell, composed of one pair of electrodes with the gaps and the buses. As for the other unit cell model, boundary conditions are imposed, simulating an infinite device (see figure 5).

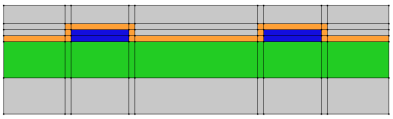

Figure 3: 2D unit cell model

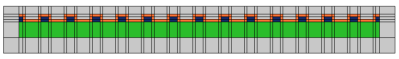

Figure 4: 2D complete model

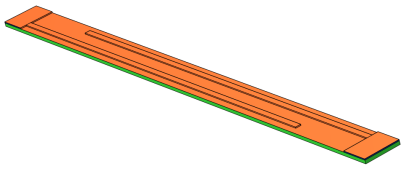

Figure 5: 3D unit cell model

On the figures above, the piezoelectric material is represented in green, the electrodes (and the reflectors) are in blue, the dielectric is in orange and the environment in grey. Notice that in figure 5, the environment is removed in order to see more clearly the device. Notice also that in this figure, electrodes are barely visible, but they are still present, between the piezoelectric and the dielectric on the bus and finger parts.

1.3 Reference parameters

In this section, we will present all the parameters that were changed during the simulations, either to study their influence on the coupling coefficient, or because they are directly correlated with other parameters that were changed (parameters that are expressed using a formula, i.e. $w_{resonator}$ and w_{finger}, are modified only because they depend on other parameters). Notice that, in table 1, the column $reference\ value$ refers to values that are generally used when one of the other parameters is changed. Therefore, when some parameters are not mentioned on a graph, one may assume that the corresponding value is the reference one.

Name	Reference value	Description
λ	3.2 μm	Width of unit cell
n (2D complete)	7	Number of pairs of electrodes
$w_{resonator}$ (2D complete)	$n * \lambda$	Width of the resonator
Duty factor	0.3	Percentage of piezoelectric covered by electrodes in a 2D-cut
w_{finger}	$duty\ factor \cdot \frac{\lambda}{2}$	Width of an electrode
t_{metal}	100 nm	Height of an electrode
$t_{dielectric}$	50 nm	Thickness of the dielectric
Aperture	30 μm	Overlap between two electrodes
t_{env}	300 nm	Thickness of the environment
Dielectric material	AlN	

Table 1: Reference parameters of the devices (listing of the different values simulated is available in table 4)

These reference values mainly come from the devices fabricated in the clean room (for example λ or t_{metal}) but others are the result of previous studies performed by the laboratory. For example, curve of coupling (without dielectric) as a function of duty factor presents a shape similar to the one of a negative square function, with maximal value observed for $duty\ factor \approx 0.38$ (see figure 6). The difference when $duty\ factor = 0.3$ is however very small, justifying therefore the choice of this value.

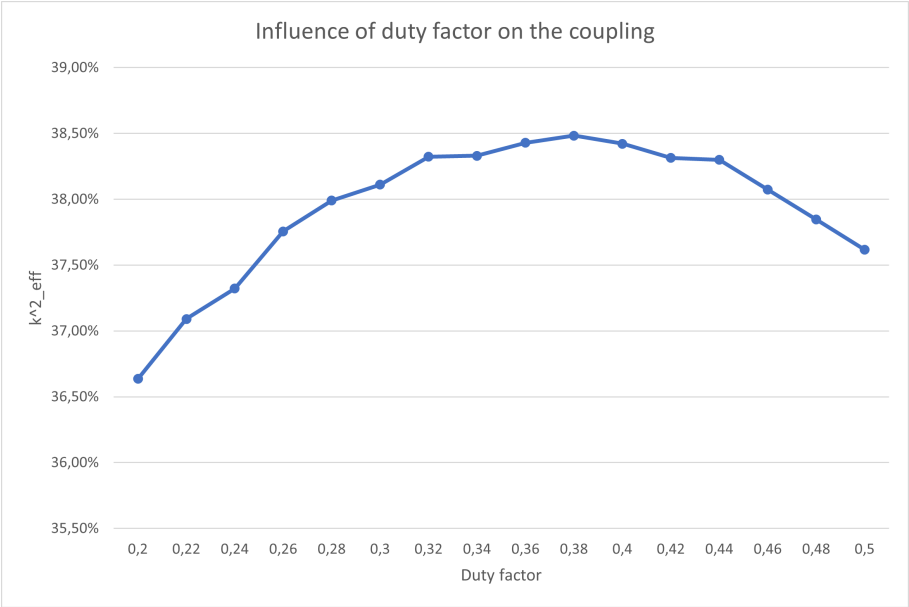

Figure 6: Plot of the coupling for different values of the duty factor, without dielectric

The rest of this report will be separated into 2 parts : the first one will present the results obtained in an environment composed of air, whereas the second one will be dedicated to the analysis of the simulations performed in an aqueous environment.

2 Simulations in air

As explained above, before starting to simulate the behaviour of the device into an aqueous environment, several studies are performed with air surrounding the resonator. Indeed, this first step helps to understand the mechanics involved, but it is also a good reference in order to verify if we observe the same trend in both environments.

First of all, it is important to know what we should observe. Recall that we are interested in the study of the shear-horizontal 0 mode. In the 2D models, it corresponds to out-of-plane displacement with directions opposed for signal and ground electrodes. For example, figure 8 shows the displacement observed at resonance for a 2D unit cell with reference parameters described in table 1 (see figure 7 for the admittance curve).

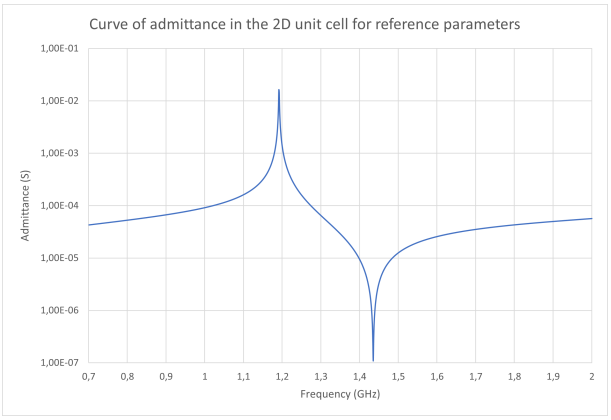

Figure 7: Initial plot of admittance for the 2D unit cell

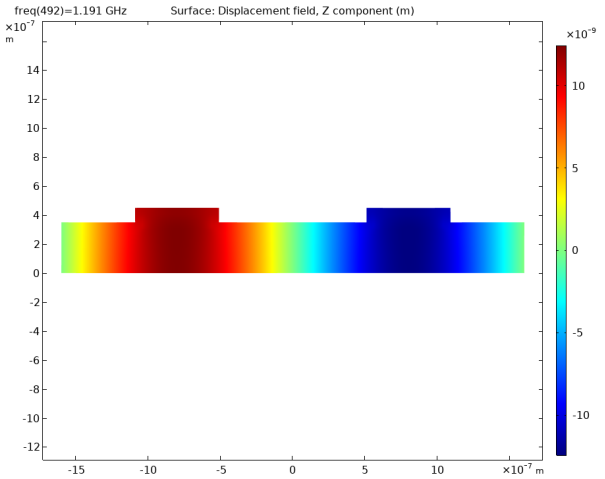

Figure 8: In-plane displacement at resonance

As the resonant frequency depends mainly on the value of λ, observing the displacement is particularly useful during the first simulations to be sure that the mode observed is the good one.

In the next section, we will present general results, i.e. results that are always observed in air when we change a given parameter, whatever the conditions.

2.1 General results

2 parameters show a same trend when they are modified : the aperture and the number of pairs of electrodes (the second one has another effect that will be described in section 2.3). Indeed, as shown in figures 9 and 10, in both cases, an increase results in an upward shift of the admittance curve, without changing its resonant and anti-resonance frequencies. The major consequence for this study is that they do not have any effect on the coupling. The reason behind this behaviour is that, when one of these parameters is increased, the total surface of overlap between electrodes of opposite polarity is also increased and this results in a higher admittance. More formally, the electrical representation (see figure 11) allows us to have a better comprehension of the mechanics involved. The parameter that evolves with the aperture and n is C_0, which characterizes the static capacitance. Therefore, it will have an effect on the entire curve.

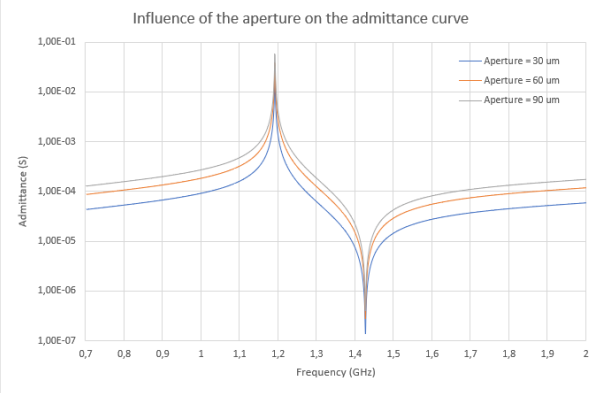

Figure 9: Plot of the admittance curve for different apertures (2D unit cell)

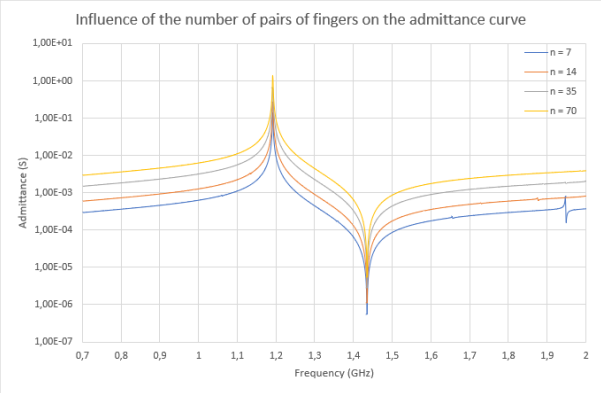

Figure 10: Plot of the admittance curve for different values of n (2D complete)

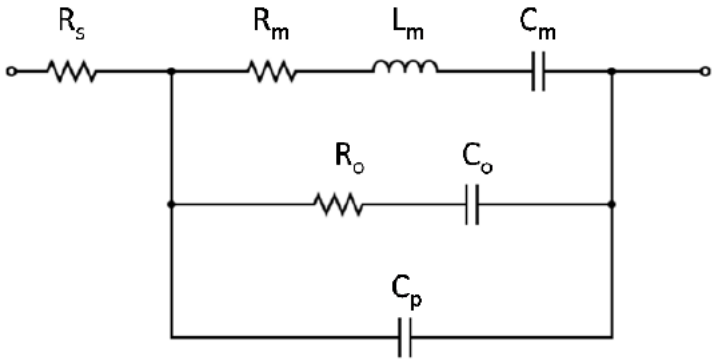

Figure 11: Electrical representation of a Lamb wave resonator [4]

Nevertheless (and fortunately), the other parameters impact the coupling of the device, therefore allowing an optimization of their characteristics. For example, an increase in t_{metal} is always associated with a reduction of both f_s and f_p (see figure 12): this is called the mass loading effect [6]. But it is also almost systematically associated with a decrease of the coupling. Indeed, the reduction of f_p is relatively more important than the one observed for f_s, particularly for small values of λ, implying thus a diminution of the coupling (the rare examples that do not follow this rule will be presented in section 2.2). Figure 13 shows this trend : for $\lambda = 3.2\ um$, curves are almost the same for both values of t_{metal}, whereas, for $\lambda = 1\ um$, we observe a $7-8$ percentage points (pp) difference. This result shows the importance of the $\frac{t_{metal}}{\lambda}$ ratio on the coupling of the device. Its effect will be discussed in more details in section 2.2.

This figure exhibits another important effect of λ on the behaviour of the resonator. Indeed, unlike t_{metal} which varies in a direction opposite to that of the coupling, the latter and λ follow the same trend. Therefore, recalling that the objective is to maximize the coupling of the device, one would say that we should take λ as large as possible. Nevertheless, section 3.1 will show that this conclusion is valid in air, but not in water. Moreover, if it is important to maximize the value of the coupling, we must recall that the objective is also to have several optimized λs and not only a unique with optimal parameters. Indeed, it is not always possible to work with the best possible λ and therefore, if for example, one wants to work around 2.5 GHz, knowing the best combination of parameters for $\lambda = 1.6\ \mu m$ is very useful.

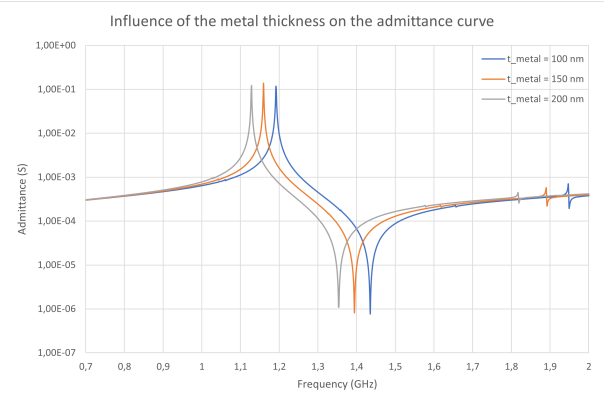

Figure 12: Plot of the admittance curve for different t_{metal} (2D complete)

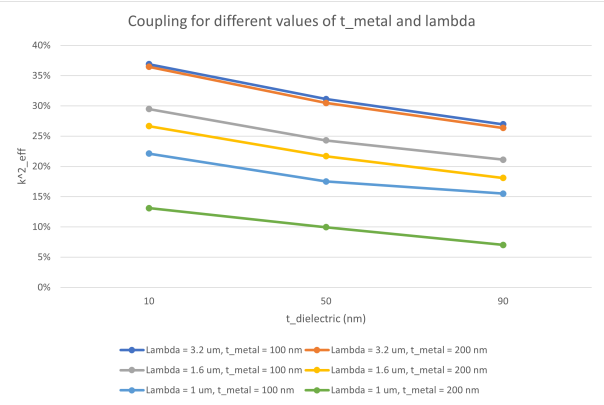

Figure 13: Plot of the coupling for different values of λ and t_{metal} (2D complete)

2.2 2D unit cell results

In this section, only results obtained using the 2D unit cell model will be presented.

The first study concerns the evaluation of the impact of a change of $t_{dielectric}$. Indeed, this parameter could be very important in an aqueous environment, as it separates it from the metal. Therefore, and even if its presence is more debatable in an environment composed of air, it will be interesting to compare its impact in both surroundings.

Figure 13, presented in the previous section, has already showed a trend of the impact of $t_{dielectric}$. Indeed, the 6 curves are associated with a decrease of the coupling when the thickness of the dielectric increases. Nevertheless, this is materialized in several ways on the admittance curve. For example, figure 14 presents lines that are gradually compressed whereas, on figure 15, some are shifted towards the left. Notice that the only parameter that is modified between these simulations is the width of the unit cell, λ. But it also affects the width of the 2 electrodes and the distance between them (see table 1 to find the expression of w_{finger}).

This last factor could in particular explain the different effects of $t_{dielectric}$ on the admittance curve. Indeed, for $\lambda = 3.2$ *or* 1.6 μm (the latter is not presented here), we observe compression of the curves when the thickness of the dielectric increases, while the behaviour is more chaotic for $\lambda = 1$ μm. This latter is associated with very small gaps between electrodes, of the same order of magnitude than the thickness of the piezoelectric, which results in highly non-linear observations, and the influence of the dielectric thickness could clearly originate from this fact.

Note that these simulations were performed using Al_2O_3 : this has no impact on the trend described, and the comparison between the 2 dielectrics will be presented thereafter.

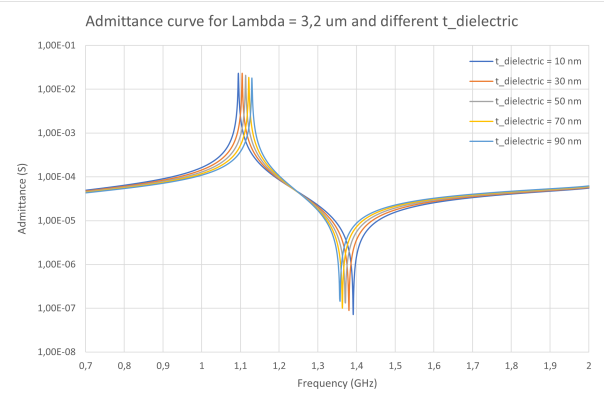

Figure 14: Plot of the admittance curve for $\lambda = 3.2\ \mu m$ and different $t_{dielectric}$ (Dielectric used : Al_2O_3)

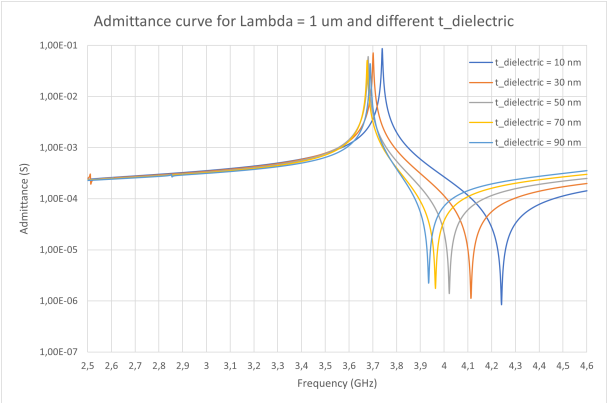

Figure 15: Plot of the admittance curve for $\lambda = 1\ \mu m$ and different $t_{dielectric}$ (Dielectric used : Al_2O_3)

In section 2.1, the influence of t_{metal} has been discussed. In particular, it has been noted that the increase of this parameter is almost always associated with a reduction of the coupling. However, for small values of t_{metal}, the coupling is approximately constant, and even slightly better for some increases of the height of the metal. This observation has led to the research of an optimal $\frac{t_{metal}}{\lambda}$ ratio for the 3 values of λ analyzed in this study, as presented in figure 16.

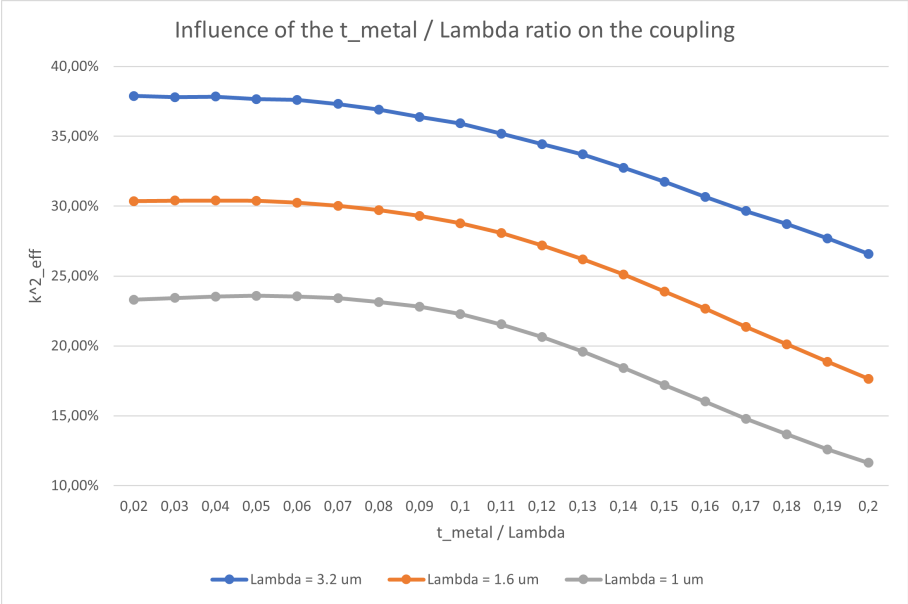

Figure 16: Plot of the coupling for different λ and $\frac{t_{metal}}{\lambda}$ ratios ($t_{dielectric} = 10\ nm$ and Dielectric used : Al_2O_3)

The 3 lines show globally the same trend with coupling approximately constant for $\frac{t_{metal}}{\lambda} \leq 0.06$. The conclusion is that, when it is feasible, one should take a value of t_{metal} such that $t_{metal} \leq 0.06 \times \lambda$, i.e. in our case, values lower than 192, 96 and 60 nm for λ respectively equal to 3.2, 1.6 and 1 μm.

So far, all simulations were performed considering an environment thickness of 300 nm. However, in real conditions, air occupies a much larger area, thus raising the question of the relevance of these results. Fortunately, we will prove that an environment composed of air has very little influence on the performance of the resonator (not negligible however).

Figure 17 shows 4 different curves of admittance obtained with the following configurations: 300 nm (1) and 1.6 μm (2) of air above the resonator, 300 nm (3) and 1.6 μm (4) of air above, but also below. The 4 lines are almost superposed, with only the part after the resonance being slightly shifted towards the left. This result is confirmed by figure 18, where the coupling is represented for these 4 configurations and different values of $t_{dielectric}$. Same shape is observed in all situations, with differences of coupling systematically lower than 1.5 pp.

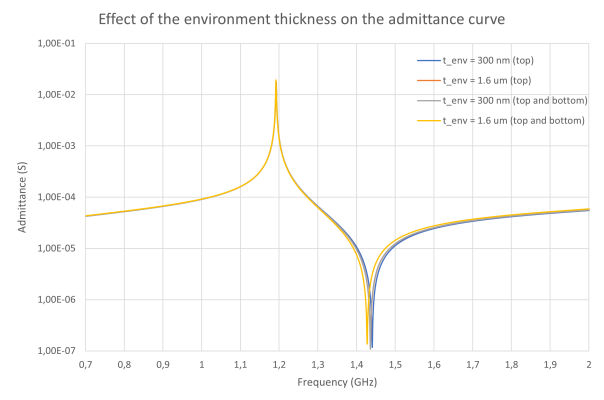

Figure 17: Plot of the admittance curve for different configurations of environment

Figure 18: Plot of the coupling for different configurations of environment

Therefore, the results previously presented are still valid but may slightly overestimate the value of the coupling.

2.3 2D complete

Previously, we have introduced some results using AlN as dielectric, and other using Al_2O_3. The main difference between these 2 materials is that the first one has a Young's modulus of 320 GPa (the choice of this value comes from [7]) while the second's is only 180 (this one comes from [8]). This is of course not the only property that differs between these 2 materials but it explains most of the changes observed during the simulations.

To be certain of this assertion, let's consider figure 19. On this graph, one should notice that the admittance curve of the device with a dielectric composed of AlN is almost equivalent to the orange one, with a shift towards the right. This observation could result from many other factors, however, the very first simulation performed with AlN (not given here) was made using a mistaken value of its Young's modulus (320 Pa instead of 320 GPa), all other parameters having the good value. The curve obtained was the same than the one presented on figure 19, but with a sharp shift to the left. Moreover, this curve also shows the impact of adding a layer of dielectric on the device : the resulting curve is compressed compared to the grey one, inducing thus a reduction of the coupling, and therefore of the performance of the resonator.

Nevertheless, this is not the only effect measurable. Indeed, the coupling is very dependent from the material used as dielectric, as shown on figure 20, but we cannot conclude that one dielectric is better than the other. For example, Al_2O_3 presents better coupling for $\lambda = 3.2$ or 1.6 μm, but becomes less efficient for a value of 1 μm.

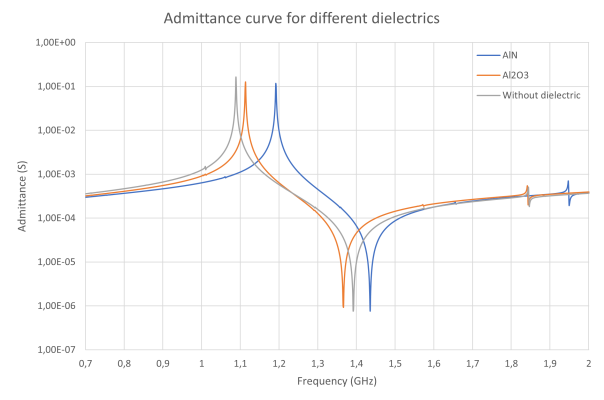

Figure 19: Plot of the admittance curve for 2 different dielectrics

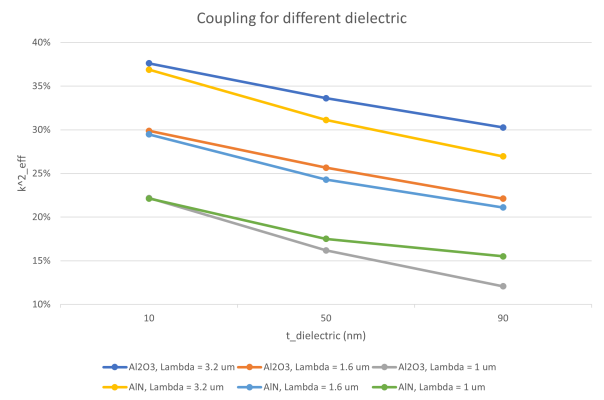

Figure 20: Plot of the coupling for 2 different dielectrics

Generally, the curves of admittance obtained in the 2D unit cell model are very smooth, with almost no perturbation. However, in the 2D complete model, more disturbances arise, particularly for some configurations. Indeed, whereas the 1^{st} one supposes an infinite number of pairs of electrodes, the 2^{nd} is finite, with reflectors at both edges that are used to reduce the losses and contain the energy within the active region of the resonator. Therefore, as the model is finite, if perturbations appear, they will be more visible (because the architecture of the device was not supposed to be optimized to reduce these disturbances).

Figures 21 and 22 show some perturbations that are very close to the resonance peak. On the 1^{st} one, little changes on $t_{dielectric}$ result in an important shift of the disturbance, moving from the left of the peak to its right. Moreover, one should note that the closer the perturbation to the peak, the higher it is. This means that it is important to confine them far from the resonance to limit their impact.

The 2^{nd} figure shows the influence of another parameter. Indeed, the only difference between the 2 graphs is the value of t_{metal} which is increased by 33%. This "little" change seems unimportant but it results in the total disappearance of the perturbation for $t_{dielectric} = 50\ nm$. Nevertheless, a new disturbance appears for $t_{dielectric} = 90\ nm$. The intuition behind this behaviour could be that, a certain "proportion" of dielectric is necessary to perturb the device, and therefore, as the weight of metal increases, more dielectric is needed to create another perturbation. The consequence is that, small changes on some parameters could be very interesting to make unwanted behaviours disappear. Another explanation for the presence of these perturbations could be that the damping used in this work is relatively small. Therefore, it will not reduce their presence, as it would be in reality (it also implies that the curves are sharper than they should be). The observation of the mode shape of the perturbations appearing in figures 21 and 22 could be very useful to determine the origin of their presence.

Notice moreover that all these perturbations arise for $\lambda = 1\ \mu m$ (in fact, it is not true, other disturbances appear for higher values of λ but they are very small compared to the ones

presented here) and that the effect of a low λ has already been discussed in section 2.2. Again, the behaviour observed in figures 21 and 22 could be the consequence of a gap between the 2 electrodes that is strongly reduced.

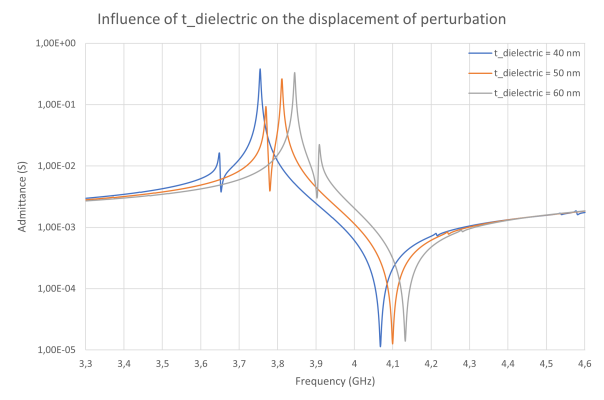

Figure 21: Effect of a change in $t_{dielectric}$ on the emplacement of a perturbation ($\lambda = 1\ \mu m$ and $t_{metal} = 150\ nm$)

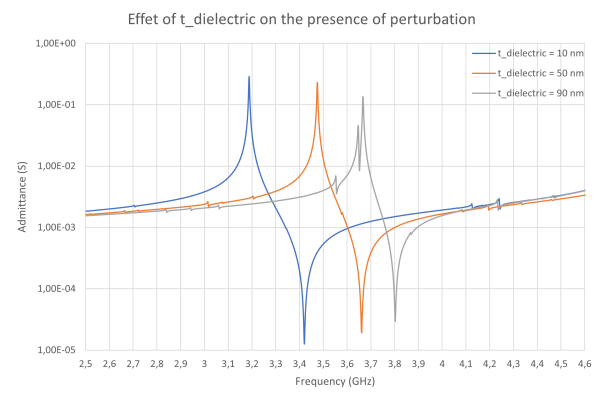

Figure 22: Effect of a change in $t_{dielectric}$ on the presence of a perturbation ($\lambda = 1\ \mu m$ and $t_{metal} = 200\ nm$)

The influence of n on the admittance curve has been briefly discussed above, in section 2.1. However, another effect arises when some conditions are fulfilled. Recall that some perturbations appear in the 2D complete model, but not in the unit cell, and that the first one considers a finite number of electrodes while the second assumes that this number goes to infinity. Therefore, we could expect that increasing n would progressively smooth the curve with disturbances that are less and less visible. To prove this assertion, we could make another simulation of the device with parameters of the middle curve in figure 21, with an increase of n from 7 to 70. The 4 curves obtained are summarized on figure 23, with a progressive disappearance of the perturbation, and almost nothing appearing for $n = 70$.

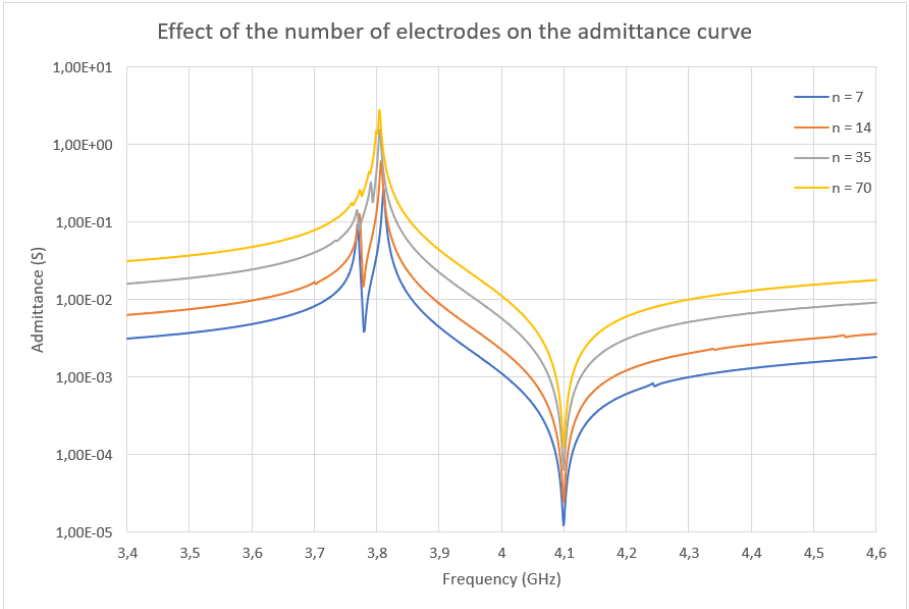

Figure 23: Plot of the admittance curve for different number of pairs of electrodes ($\lambda = 1\ \mu m$ and $t_{metal} = 150\ nm$)

2.4 Comparison of 2D models

So far, we have analyzed some results obtained using 2 different models : a 2D unit cell and a 2D complete. However, we have not yet focused on the comparison between these 2 models. In this section, we will verify if both give similar results.

In figure 24, curves of admittance obtained for different t_{metal} are presented. One should note the difference of amplitude between the 2 models. Indeed, all the curves for the finite device are approximately one order of magnitude higher than the ones obtained with the unit cell. This result seems contradictory with the description given in section 2.1 of the effect of the number of pairs of electrodes on the admittance curve. However, even if the 2D unit cell model supposes an infinite repetition of the cell, it does not take into account the number of pairs to compute the static capacitance C_0. Therefore, C_0 corresponds to the static capacitance of a device composed of a single pair, and it is coherent to observe higher admittance in the 2D complete model. Moreover, in both models, the same value of aperture is used because it strongly impacts the resulting capacitance. Therefore, the explanation is still valid.

Nevertheless, despite this difference, we should notice a very good accuracy of resonant and anti-resonance frequencies from one model to another, with very slight differences. Curves are therefore simply shifted upwards with almost no other incidence on the behaviour of the resonator. Figure 25 confirms this result with a comparison of coupling for different λ : for $\lambda = 3.2$ or 1.6 μm, the coupling is almost equal, whereas for $\lambda = 1$ μm, the lines are even superposed. This again shows the very good agreement between the 2 models, which tends to be even better when λ is reduced.

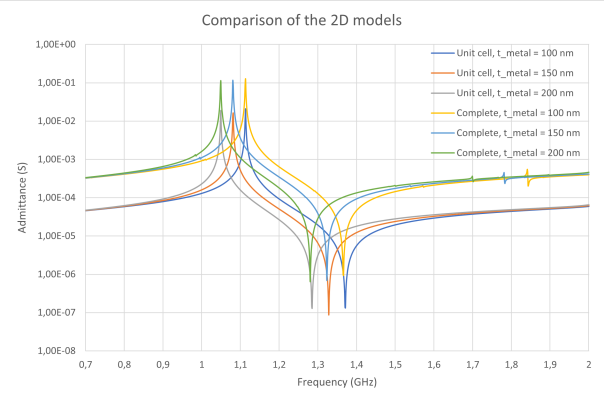

Figure 24: Plot of admittance curves obtained with the 2D models (Dielectric used : Al_2O_3)

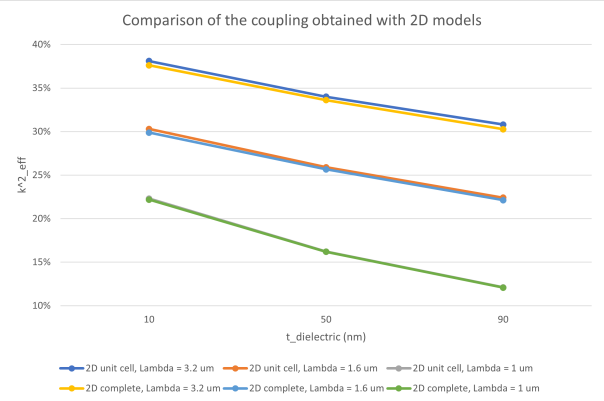

Figure 25: Plot of the coupling obtained with the 2D models (Dielectric used : Al_2O_3)

However, as explained above, some perturbations arise in the 2D complete model and not in the unit cell. If we take again the values of example described by figure 23, and plot the curves obtained in 2 models, we clearly see that the first one is perfectly smooth while the other one presents a disturbance close to the peak. Nevertheless, despite this perturbation, resonant and anti-resonance frequencies are again very close. Therefore, we can again insist on the very good agreement between the couplings obtained in these 2 models. Thus, using the 2D unit cell model could be very interesting in future simulations, given the high accuracy of the results, and the reduction of computational time.

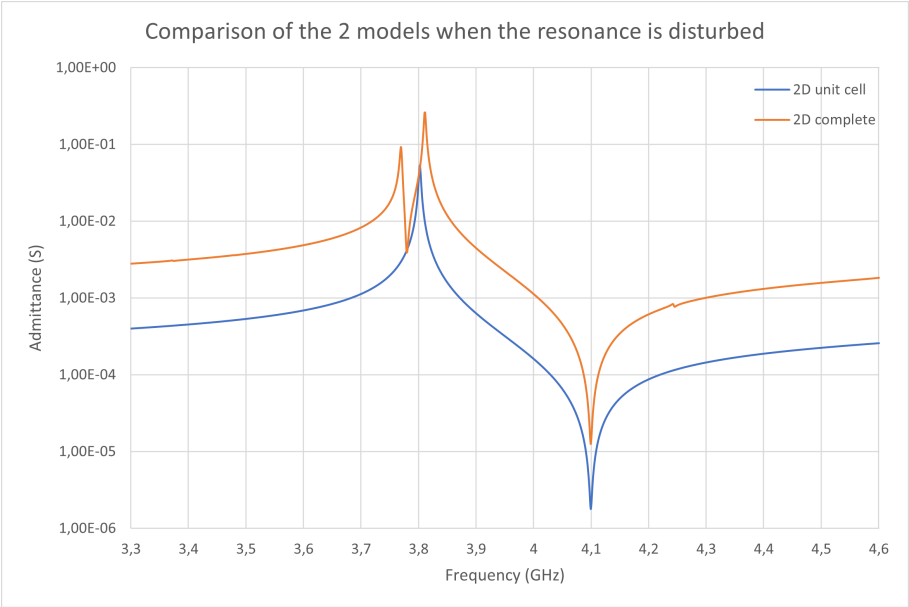

Figure 26: Comparison of the 2 models when there is a perturbation ($\lambda = 1\ \mu m$ and $t_{metal} = 150\ nm$)

2.5 3D unit cell

Even if only a few simulations have been performed on the 3D unit cell, it will be very interesting to compare the results with what we have obtained so far. Many questions arise: do the admittance curves conserve the same global shape ? Do we observe the same trends than before when a parameter is modified ? Are the values of coupling constant from one model to another ?

Previously, the effect of the Young's modulus on the resonant and anti-resonance frequencies has been demonstrated. Indeed, dielectrics with higher Young's modulus tend generally to have a shift towards the right of their admittance curve. Figure 27 shows the same global trend in 3D, but presents also a noticeable difference : lots of perturbations appear between the resonant and anti-resonance frequencies. These modes are recurrent in 3D (but also in reality) and are called "spurious modes". Many factors are involved in the apparition of these modes, but only 2 of them will be quickly presented. Joab R. Winkler and J. Brian Davies have shown that a main cause of these modes is a system excessively flexible [9]. Indeed, the fingers we analyze here are very thin, and therefore subject to strong displacements. But this is not the only reason explaining the presence of these transverse modes. M. Solal et al have discussed the influence of the electrode end gaps on their apparition and shown that the reflection of the wave in these regions creates perturbations characterized by the spurious modes [10].

These spurious modes are unwanted because they can lead to very inaccurate estimations of the coupling coefficient. In 2019, R. Lu, M. -H. Li, Y. Yang, T. Manzaneque and S. Gong have shown that, depending on the location of the spurious mode, the anti-resonance frequency could be under or overestimated: a spurious mode with resonant frequency lower than the anti-resonance frequency of the resonator will push this latter to the right, while a reversed situation will push the anti-resonance frequency to the left [5]. That's why many studies have been performed to suppress these transverse modes (it is however not the objective of this semester project). For example, paper [10] evoked above has demonstrated an important reduction of the spurious modes when pistons are added at the end of the fingers, without much effect on

the coupling.

Even if these transverse modes induce inaccurate estimations of the coupling, it is interesting to compare the curves obtained in the 2 unit cell models. Figure 28 shows the admittance curves for the reference parameters. First, we should note the presence of the spurious modes between the resonant and anti-resonance frequencies in the 3D model, but not in 2D, as expected. Second, the very good concordance before the resonance, and after the anti-resonance is remarkable. The most surprising is that, in the 2 models, f_s and f_p are almost equal, leading to a contradiction with the explanation given on the effect of the spurious modes. A possible reason is that the coupling coefficients deduced from 2D results could be overestimated. Therefore, the real anti-resonance frequency would be smaller and the 3D model result would be coherent with what is expected. Another possibility is that, as the last spurious mode appears just after the anti-resonance frequency, it could compensate the effect of the other spurious modes. Finally, recalling that the damping is relatively small, maybe the amplitude of the spurious modes is exaggerated on this figure and their effect should be less important than one could expect when observing the figure.

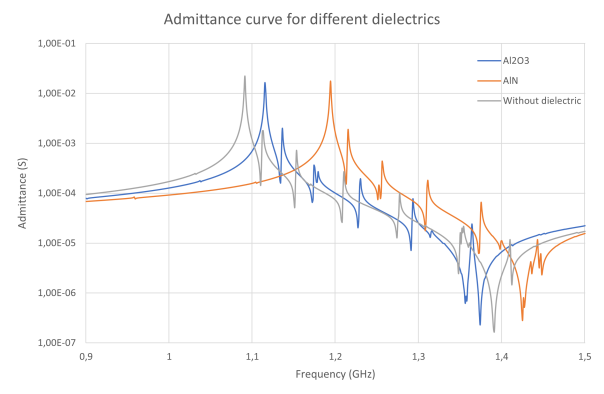

Figure 27: Comparison of the dielectrics used

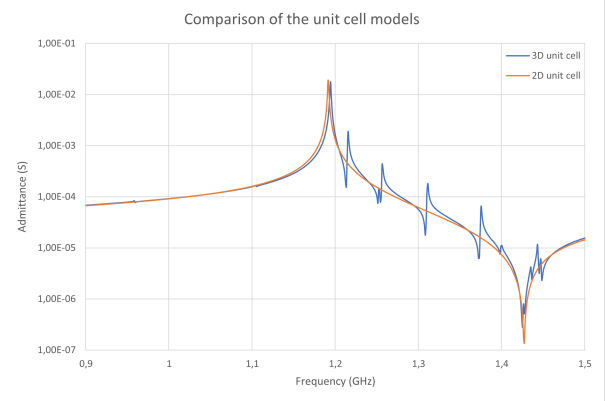

Figure 28: Comparison of the admittance curves for unit cell models

This section closes the discussion on the simulations in air. The rest of this document will now focus on the simulations in water.

3 Simulations in water

Please, notice that in water, the reference value of the thickness environment is 1.6 μm and not 300 nm anymore. Indeed, as it will be demonstrated later, thickness of water influences strongly the coupling. Therefore, if no indication is given on t_{env} in this section, one may assume that it is equal to 1.6 μm (this value was chosen because it corresponds to half the largest λ).

Moreover, given the strong impact of water on the behaviour of the resonator, no section will focus on general results, as it was done for simulations in air. Indeed, again, the following simulations will show that no global trend can be extrapolated when a parameter is changed, because the result depends highly on the other parameters.

Finally, before moving to the next section, recall that the objective of this project is not only to find the best possible coupling, but to find an interesting combination of parameters for all values of λ. Therefore, even if the next sections will sometimes refer to a unique optimal combination, section 3.5 will give the best combinations for all λs.

3.1 2D unit cell

Before entering into the details, it is interesting to compare 2 simple curves of admittance for a device placed first in air, and then in water, in order to better understand the effect of the aqueous environment on the coupling.

Figure 29 shows a comparison when reference parameters are used (recall that in water, reference thickness of the environment is 1.6 μm). The 2 curves are very different: first, resonant and anti-resonance frequencies are reduced when the device is surrounded by water. Second, the reduction in anti-resonance frequency is much more higher than the one observed for the resonance, thus inducing a strong diminution of the coupling. Third, the amplitude of the admittance curve is also reduced with peaks that are smaller than the ones observed in air. Finally, it is important to keep in mind that the same value of damping has been used in both environments, while, in reality, it would be higher in water, and the curves would therefore be less sharp (because the quality factor would be reduced).

Thus, as expected, the performance of the resonator will be reduced in an aqueous environment and we should observe this same behaviour in the next simulations.

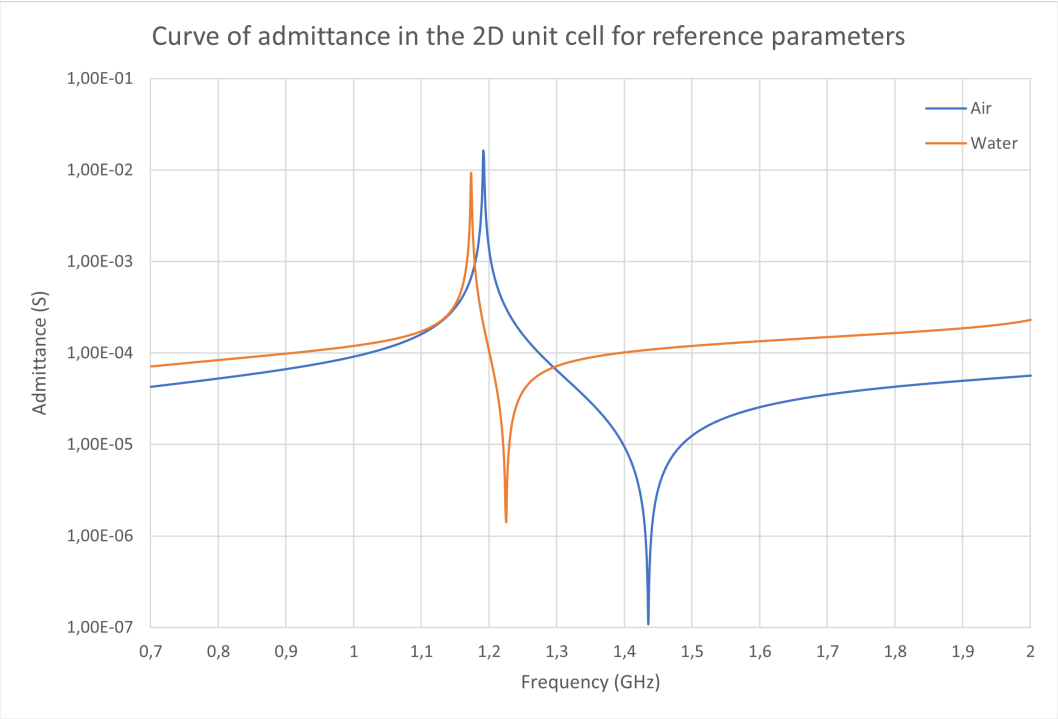

Figure 29: Comparison of the reference curves in air and water

The first analysis will focus on the influence of λ and $t_{dielectric}$ on the coupling coefficient. Figure 30 shows the evolution of the coupling when these 2 parameters are modified. The main difference with the result obtained in air is that we do not observe a reduction of the coupling with the diminution of λ. Indeed, we even notice the opposite trend with a coupling that is higher for low values of λ. This behaviour could be explained by the fact that the exchanges between electrodes occur mainly across the environment. Therefore, the more space between the electrodes, the more reduction in the coupling. However, when λ is reduced, the gap follows the same trend and it generates less losses. The diminution of the coupling induced by the reduction of λ is thus compensated (and even more) by the gap reduction.

Concerning the thickness of the dielectric, again the behaviour differs from what was previously observed. Indeed, for small values of $t_{dielectric}$ $(10 - 20\ nm)$, we observe an improvement of the resulting coupling. Moreover, even when the thickness of the dielectric increases beyond these values, the coupling is still higher than the one obtained without dielectric (until 70 nm for $\lambda = 1$ or 1.6 μm and until 50 nm for $\lambda = 3.2\mu m$). The reason is that both the environment and the dielectric are noxious for the performance of the resonator but the second one induces less degradation than the first one. However, as $t_{dielectric}$ increases, the coupling diminishes because, when a certain quantity of dielectric is attained, the device is sufficiently separated from the environment and adding more dielectric will not generate a sufficient extra-protection to increase the coupling.

Given the shape of the curves, a combination ($\lambda = 1\ \mu m$, $t_{dielectric} = 20\ nm$) is therefore recommended for a device working in an aqueous environment.

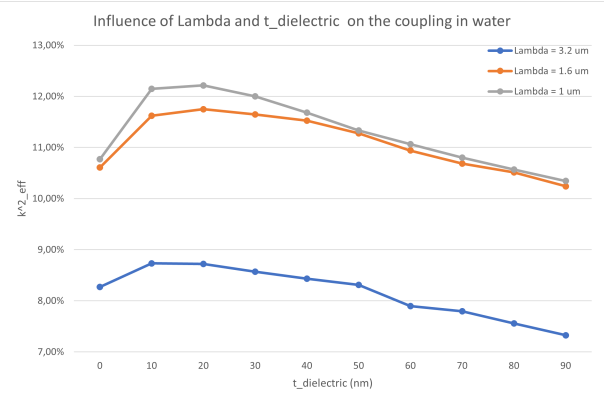

Figure 30: Coupling as a function of λ and $t_{dielectric}$ in water

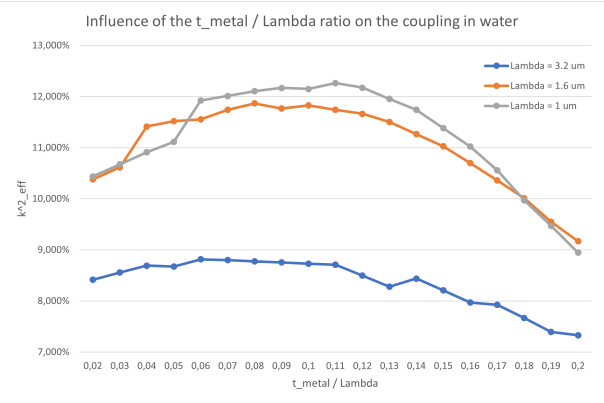

Figure 31: Plot of the coupling for different λ and $\frac{t_{metal}}{\lambda}$ ratios ($t_{dielectric} = 10\ nm$)

Figure 31 shows the coupling obtained for different λs when the ratio $\frac{t_{metal}}{\lambda}$ is changed. If we observe a similarity with the result given in figure 16 (an increasing/constant coupling for small values of the ratio and then a decrease), there are also some major differences. Indeed, the first one is that, the increase in coupling is much more stronger and happens for more values of $\frac{t_{metal}}{\lambda}$ than what we had in air. The second one is that, whereas in air, the curves seemed simply shifted toward the top or the bottom, here they differ from each other and a global trend cannot be described. Indeed, for $\lambda = 3.2\ \mu m$, the coupling slightly increases, then stays constant and finally decreases, while for $\lambda = 1.6\ or\ 1\ \mu m$, it strongly increases, reaches a maximum for respectively $\frac{t_{metal}}{\lambda} = 0.08$ and 0.11 and then decreases. Moreover, the curves of the smallest λs cross each other 2 times, indicating a clearly non-linear influence of these latter on the effect of the ratio. However, a best choice of duo (λ, $\frac{t_{metal}}{\lambda}$) can be chosen and is given by (1 μm, 0.11).

So far, simulations in water have been performed using $t_{env} = 1.6\ \mu m$ and considering an environment at top and bottom. Now, the influence of thickness and localisation of this environment will be analyzed to better understand these choices. First, figure 32 presents 4 different environment configurations : water above and below the resonator, water above and air below, water above only, and finally air above and below. If the curves of water above and air or nothing below are almost superimposed, adding a layer of water below the device induces a strong change of the admittance curve. Indeed, resonant and anti-resonance frequencies (in particular the second one) are reduced: this means that, even if the electrodes mainly exchange energy through the top part of the device, the bottom environment also plays a major role. Moreover, we should again notice the strong differences happening when a device is placed in air or in water. That's why it is very important to reduce as much as possible the impact of water on the resonator.

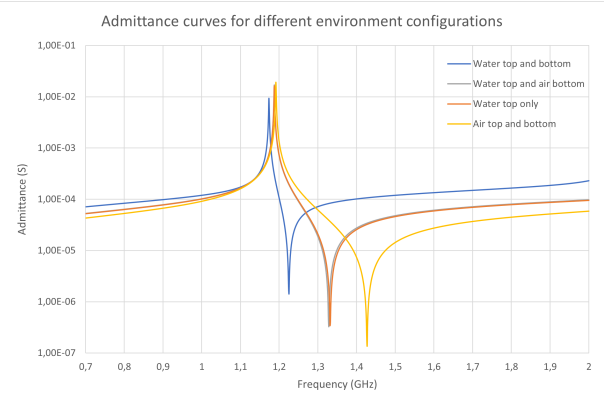

Figure 32: Influence of the environment on the admittance curve ($t_{env} = 1.6\ \mu m$)

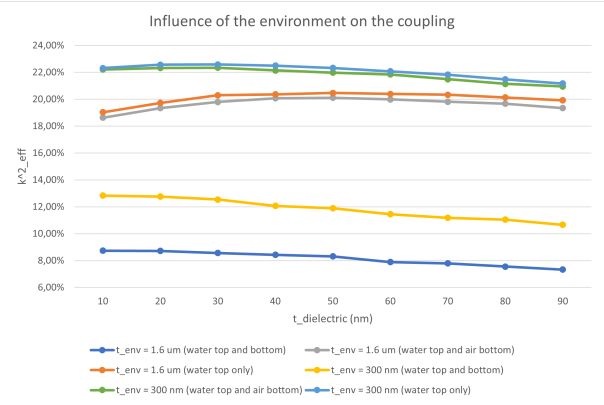

Figure 33: Coupling for different environment configurations

Similarly, figure 33 presents 6 different configurations: water above and below the device, water above and air below, and finally water above only, for $t_{env} = 1.6\ \mu m\ or\ 300\ nm$. Let's first compare the impact of the thickness environment: while for a medium composed of air, the thickness had almost no effect on the coupling, in water a difference of almost 4 *pp* is observed from $t_{env} = 1.6\ \mu m\ to\ 300\ nm$. That's why one cannot assume a small layer of environment. Moreover, the graph shows again the small difference induced when air is adding to the surrounding, particularly compared to the impact made by adding a layer of water. Indeed, we observe a difference of about 10 *pp* from the configuration with water above only to the one with water below. All these results have led to the choice of the actual configuration.

We will now focus on the effect of duty factor on the performance of the device. First, recall that the value of 0.3 was chosen because of previous studies performed in the laboratory in an environment composed of air, and without dielectric. As shown by figure 34, this result is however not transposable to the aqueous medium. Indeed, the curves are monotonously increasing till a value of duty factor about 0.54 is attained. For all λs, the coupling increases by approximately 1.6 *pp* from $duty\ factor = 0.3$ to 0.54, which is very substantial given the low values of coupling obtained in water. This difference with the result in air could again be explained by the perturbations provoked in water. Indeed, an increase of duty factor generates a reduction of the space between electrodes, therefore reducing the volume of water separating them. However, when electrodes become too close, other perturbations deleterious for the behaviour of the resonator appear, explaining why a plateau is reached for $duty\ factor = 0.54$.

Moreover, again, curves for $\lambda = 1\ and\ 1.6\ \mu m$ cross each other (but only one time). An explanation for this behaviour could be that the second curve benefits more than the first one of the increase in duty factor. Indeed, as the gap between electrodes is larger, perturbations are less likely to appear. Therefore, while a value of λ equal to 1 μm was previously recommended, it's not the case anymore here. However, given the slight differences between the 2 couplings, we will keep this value of $\lambda = 1\ \mu m$ for the moment and analyze later if this result still makes sense.

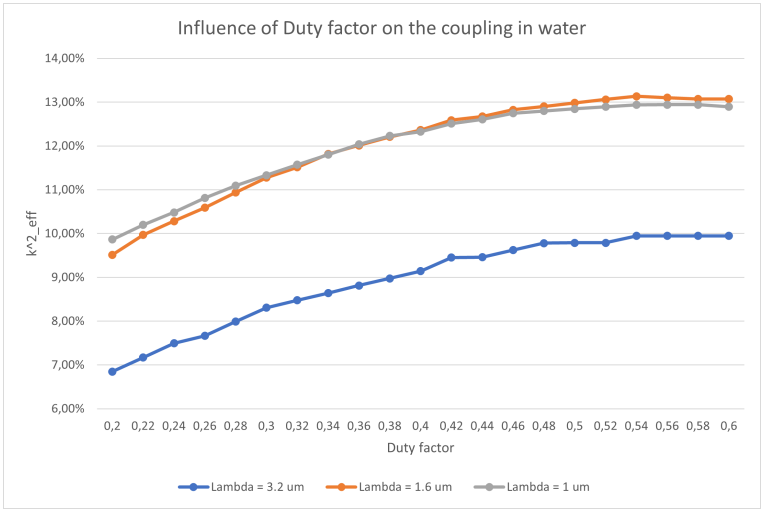

Figure 34: Coupling as a function of λ and duty factor in water

Before moving to the next section, a last analysis will be presented in the 2D unit cell model. This one is exclusive to the aqueous environment because it doesn't make sense in air. Indeed, recall the large differences in coupling induced by the presence of water under the piezoelectric (see figure 33). This has raised a question about the possibility of adding a layer of dielectric to separate the piezoelectric and the water under the device.

We know that increasing the layer of dielectric at the top of the device leads to a shift of the admittance curve towards the right. So, a similar result could be expected when a layer of dielectric is added at the bottom. Figure 35 confirms this trend but this is not the only impact of this extra-layer of dielectric. Indeed, figure 36 shows a very interesting fact : for all values of $t_{dielectric}$, this new layer results in an increase of the coupling, independently of the value of λ. The difference between the 2 configurations (with and without the bottom layer of dielectric) is even increasing with $t_{dielectric}$ for the 2 larger values of λ while it is approximately constant for the smaller value. Again, the configuration with $\lambda = 1.6\ \mu m$ becomes more interesting for some values of $t_{dielectric}$. However, the duo ($\lambda = 1\ \mu m$, $t_{dielectric} = 20\ nm$) is still the best combination of parameters with an increase of the coupling of 0.77 pp. Nevertheless, given the difficulty of adding the dielectric below the piezoelectric, it is unlikely to be implemented.

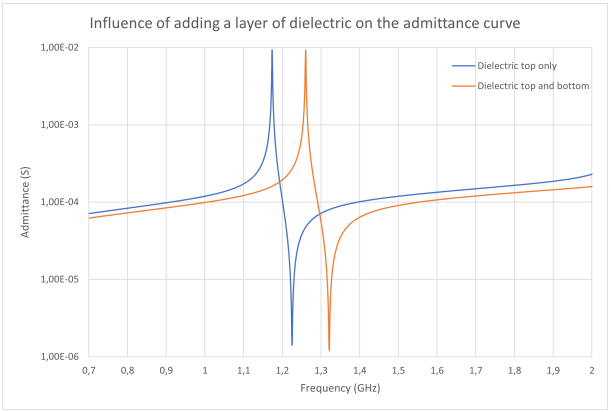

Figure 35: Comparison of the admittance curves when a layer of dielectric is added

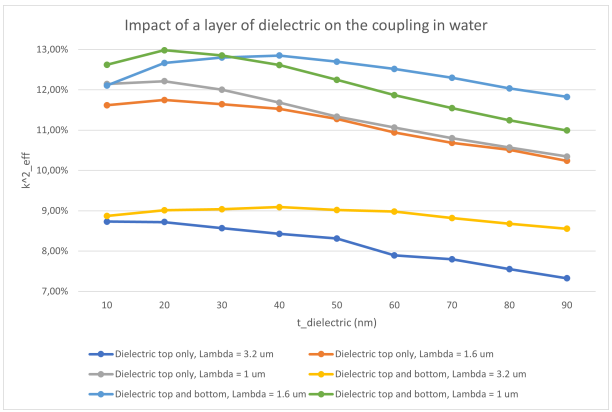

Figure 36: Impact of adding a layer of dielectric on the coupling in water

The next section will now focus on the results observed using the 2D complete model

3.2 2D complete

The first analysis to be performed is the comparison of the 2 dielectrics : AlN and Al_2O_3. Figure 37 shows the 2 admittance curves for the reference parameters. But, before comparing them, one should note the differences between figure 35 and 37. Indeed, both figures present the curve for AlN with reference parameters but they differ partially. Indeed, if the parts containing the resonant and anti-resonance frequencies are very similar, we observe strong perturbations after the SH0 mode, that were not visible in the unit cell model. These differences will be investigated in more details later on.

If we go back to the comparison of the 2 admittance curves on figure 37, the result is similar to what was observed in air, with the curve of AlN on the right. Again, this shows the effect of increasing the Young's modulus of the material. But the more interesting results are given by figure 38. Indeed, first, Al_2O_3 is globally a better dielectric than AlN, as it induces a lower reduction of the coupling. It is also interesting to notice that the curves for the 2 dielectrics do not follow the same trends. For example, for $\lambda = 3.2\ \mu m$, coupling diminishes with $t_{dielectric,AlN}$ while it is first increasing and then approximately constant until a value of 50 nm is attained for $t_{dielectric,Al_2O_3}$. But the most surprising is that, for Al_2O_3 and $\lambda = 1\ \mu m$, a net performance drop is observed, leading to a dielectric finally less efficient than the other for $t_{dielectric} \geq 70\ nm$. It is difficult to determine exactly the phenomena producing this effect, but one reason could be that again, the reduction of λ produces very high nonlinearities.

Despite all these results, figure 38 confirms the best duo (λ, $t_{dielectric}$) given above.

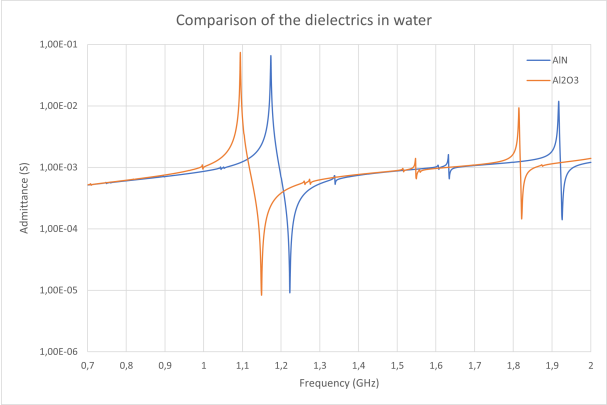

Figure 37: Admittance curves for the 2 dielectrics in water

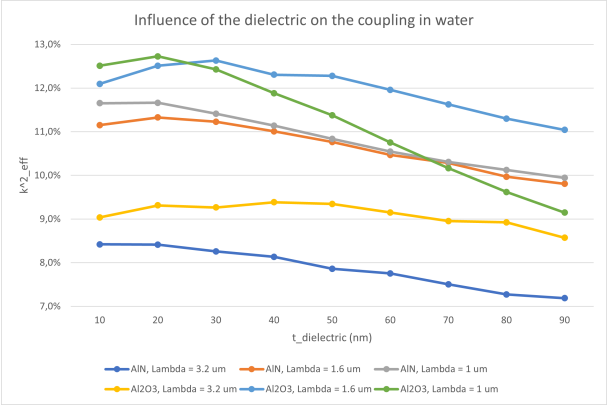

Figure 38: Comparison of the 2 dielectrics in water

Another important parameter for the 2D complete model that has not yet been discussed in water, is the influence of the number of electrodes. In air, their only impact was to shift upward the curve of admittance and reduce the perturbations but in water, another effect appears. Indeed, if the upward shift is still present in figures 39 and 40, one should notice that there is also a slight shift toward the right, in particular for the anti-resonance frequencies. This means that it also impacts the resulting coupling of the device, even if the effect is small. Therefore, increasing the number of pairs of electrodes results in a slight increase of the coupling. Figure 41 shows more clearly this effect with a gain of about 1 pp for $\lambda = 1\ \mu m$ from $n = 7$ to $n = 70$, which is substantial. However, it is also important to keep in mind 2 facts :

- First, the environment of this device is a cell, which is very small and limits the maximum number of electrodes one could implement.
- Second, increasing n implies that the fabricated device is brittler.

Therefore, as for many other parameters, the choice of n depends on compromises one should make.

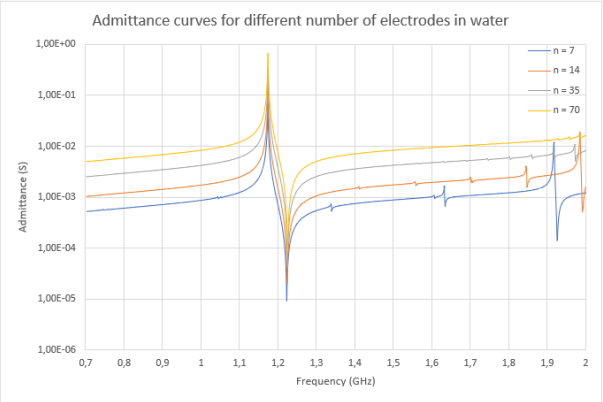

Figure 39: Admittance curves for different n in water

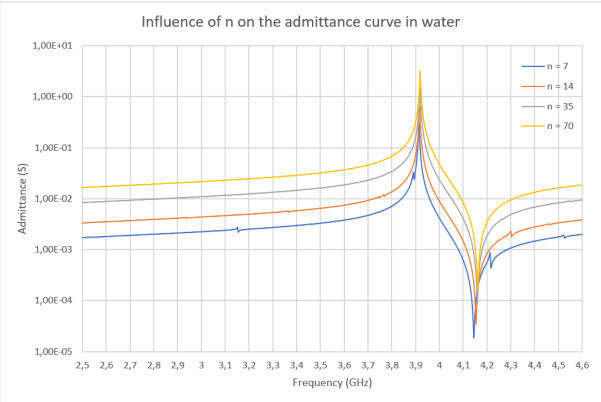

Figure 40: Admittance curves for $\lambda = 1\ \mu m$ and different n in water

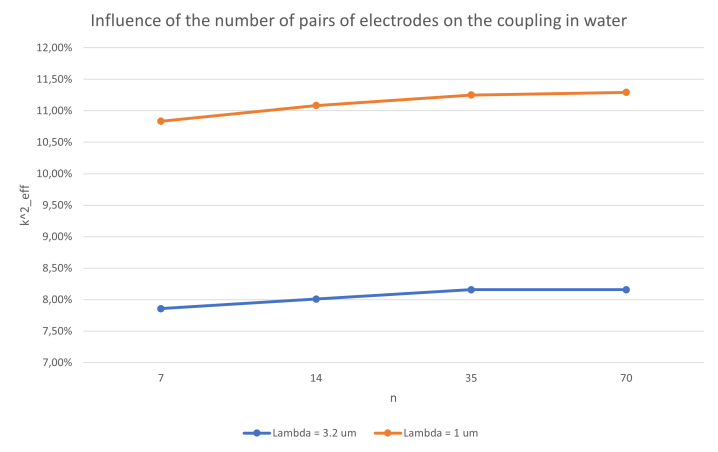

Figure 41: Effect of a change of the number of pairs of electrodes on the coupling in water

3.3 Comparison of 2D models

Recall that in air, there was a very good agreement between the 2D models. This section will investigate if this result holds when the environment is composed of water. Figure 42 shows the curves obtained with the reference parameters. They have already been briefly discussed above but they were not on the same graph. Here, one should note that resonant and anti-resonance frequencies are almost equal, with the last one slightly lower in the 2D complete model. But, as discussed above, the main difference appears after the SH0 mode, where disturbances arise on the 2D complete model, while the curve for the unit cell is very smooth. This shows that again, the complete model highlights much more phenomena than the unit cell, because of the reflection of the wave on the reflectors.

Figure 43 shows the same comparison, but with $\lambda = 1\ \mu m$. If both curves follow the same trend, we see more differences than in the first graph. This could result from the higher frequencies involved. Indeed, as the resonant and anti-resonance frequencies are multiplied by 3 to 4 compared to the other figure, a same difference (in percentage) is more visible. But this could also results from the nonlinearities happening when λ becomes too small. However, even if the difference is more noticeable, it still seems reasonable as a first approximation.

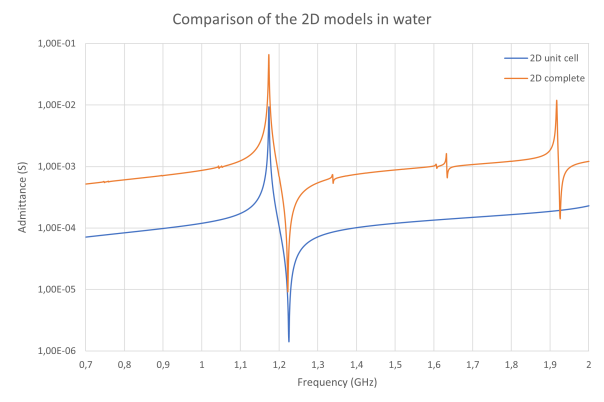

Figure 42: Comparison of the admittance curves for the 2D models in water (reference parameters)

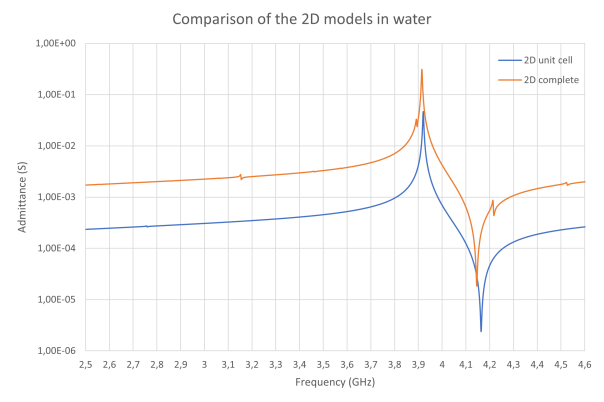

Figure 43: Comparison of the admittance curves for the 2D models in water when $\lambda = 1\ \mu m$

Figure 44 finally shows the resulting coupling in both models as a function of λ and $t_{dielectric}$. Globally, the curves follow the same trend (in particular, performances for $\lambda = 1.6\ and\ 1\ \mu m$ become very close when the thickness of the dielectric is important) but, while in air, they were almost superposed, here there is always a difference (between 0.5 and 1 pp for $\lambda = 1.6\ or\ 1\ \mu m$ and lower than 0.5 pp for $\lambda = 3.2\ \mu m$). The unit cell always tends to slightly overestimate the coupling, in particular for small values of λ but again, it shows that in a first approximation, it is a very good estimation of the coupling.

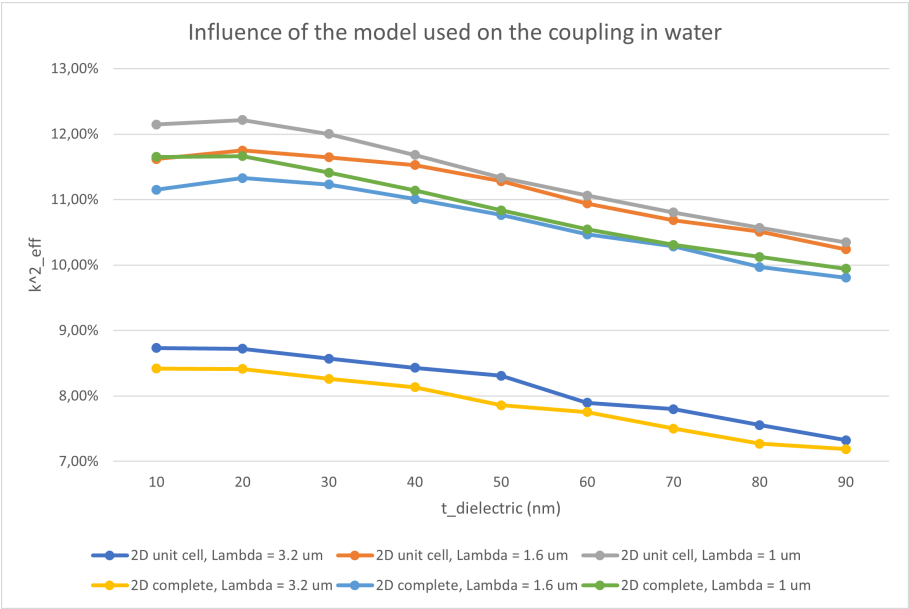

Figure 44: Comparison of the coupling for the 2D models in water

3.4 3D unit cell

In section 3.1, the influence of the environment on the admittance curve and the coupling of the resonator has been discussed. However, it is even more important to analyze its impact in 3D, where much more perturbations arise. Figure 45 compares 3 different configurations : air above and below the resonator, water above and air below, and finally water above and below. Again, a strong reduction of the coupling is observed but it is also associated to a change of spurious modes. From the first configuration to the second one, 2 spurious modes disappear (1 between the resonant and anti-resonance frequencies and 1 after the second one), while another one disappears when switching to the last configuration. Indeed, even if water has a noxious effect on the resonator, the strong reduction of the coupling induces that both resonant and anti-resonance frequencies become very close. Therefore, there is "less space" for spurious modes to develop and the few that remain are very close from one to each other.

However, it is also more complicated to deduce the true value of the anti-resonance frequency. Indeed, a spurious mode appears next to the anti-resonance frequency and therefore it is difficult to assert if the good one is the first or the second. In reality, it is probably between them, but it shows again the difficulty to work with spurious modes and the necessity to eliminate them.

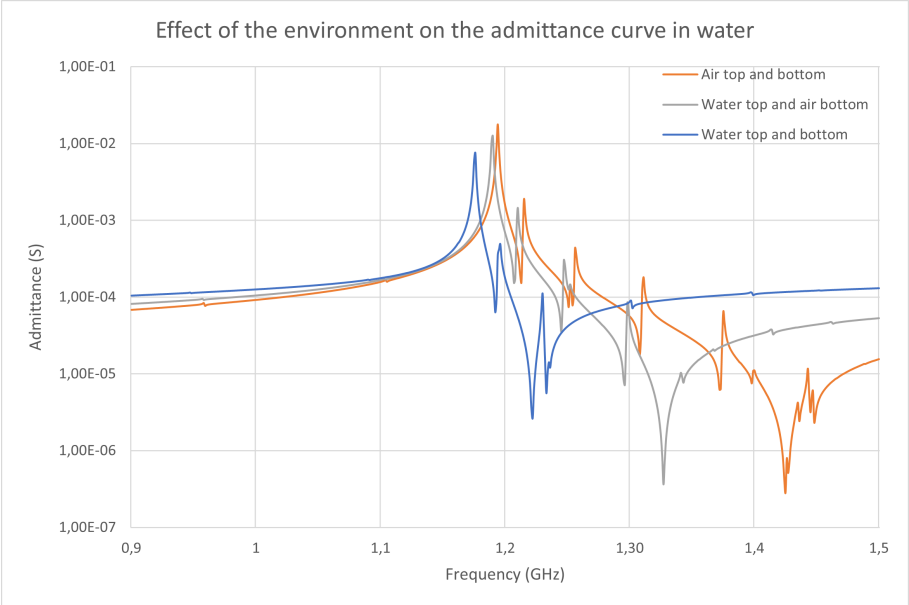

Figure 45: Comparison of the admittance curves obtained for different environment configurations

Figure 46 compares the admittance curves obtained in both unit cell models. Again, if spurious modes are considered apart, a very good agreement is observed, with very close resonant and anti-resonance frequencies and a similar global trend observed. This is again surprising as the spurious modes should shift the anti-resonance frequency and thus lead to more differences than what is observed. However, recall that a spurious mode before the anti-resonance frequency shifts this latter to the right while a spurious mode after induces the contrary. Here, one spurious mode happens clearly between the resonant and anti-resonance frequencies whereas the other one seems to occur after. Therefore, it is possible that both modes compensate each other and lead to a good estimate of the anti-resonance frequency. However, as it is difficult to know which down peak corresponds to the spurious mode and which one corresponds to the real anti-resonance frequency, this explanation could also be wrong.

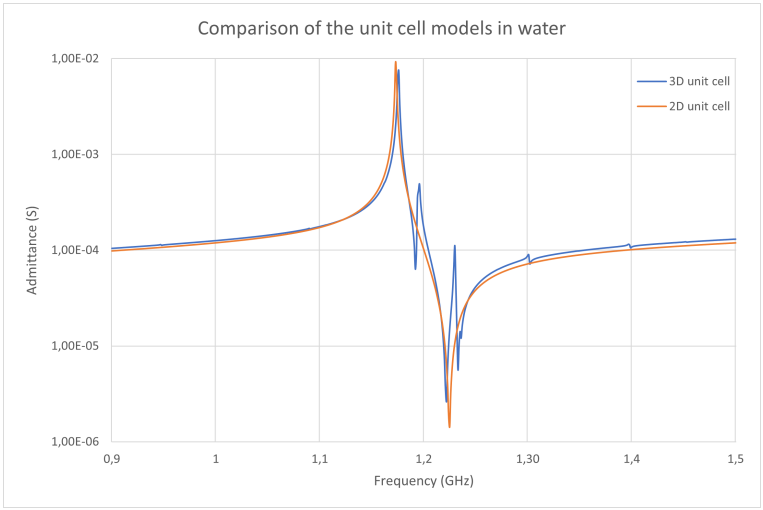

Figure 46: Comparison of the admittance curves obtained with the unit cell models

Recall that earlier, an optimal duty factor value was found to be 0.54 : it allowed a maximized coupling coefficient for $\lambda = 1\ \mu m$. However, it has also be shown that the closer the electrodes are from each other, the more perturbations appear. Therefore, it would be interesting to verify the shape of the admittance curve when this new value of duty factor is imposed. Figure 47 compares the admittance curves when only duty factor is modified. First, one clearly sees that the coupling coefficient is, as expected, higher for this new configuration. Indeed, anti-resonance frequencies are almost equal while a shift towards the left of the resonant frequency is observed when $duty\ factor = 0.54$. Moreover, the perturbation that was observed on the right of the anti-resonance frequency appears now between the 2 peaks, and could thus lead to an overestimate of the coupling coefficient. Finally, if the spurious modes have an amplitude slightly higher for the new duty factor, they are however still reasonable and no real increase of their presence is noticeable.

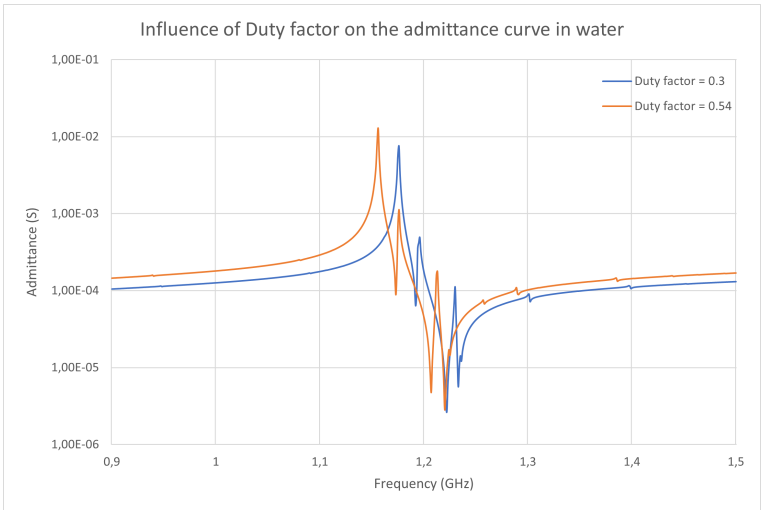

Figure 47: Comparison of the admittance curves for reference and optimal duty factors

Now that all these results have been presented and discussed, it will be interesting to verify if an optimal coupling coefficient can be found. Next section will be dedicated to the search of such a k^2_{eff}.

3.5 Recommendation

In previous sections, it has been shown that, by modifying some parameters, the resulting coupling can be modified, either positively or negatively. Therefore, it is possible to optimize these parameters in order to obtain a value of k_{eff}^2 as high as possible. But, even if it is important to find this value, one must also recall that it is sometimes not possible to work with a given value of λ. That's why this section will be dedicated to the research of the highest value of k_{eff}^2, but also of the maximum coupling for all values of λ investigated so far.

Sections 3.1 and 3.2 have allowed to find a first candidate for the best coupling achievable with this device (parameters are summarized in table 2). We will first compare the curves obtained for the reference parameters and this candidate, and then verify if a better coupling is achievable.

Name	Reference value	First candidate
λ	3.2 μm	1 μm
Duty factor	0.3	0.54
t_{metal}	100 nm	110 nm
$t_{dielectric}$	50 nm	20 nm
Dielectric material	AlN	Al_2O_3
n (2D complete)	7	70

Table 2: Ideal parameters for the device

Because of the strong influence of λ on the resonant and anti-resonance frequencies, it doesn't really make sense to compare the curves obtained with 2 different λs. Therefore, the admittance curves will be compared, but using the same value of λ equal to 1 μm. In particular, figure 48 presents 5 different configurations: reference parameters without dielectric, reference parameters with AlN and Al_2O_3 and first candidate with and without dielectric below the piezoelectric. Notice that these curves were obtained using the 2D unit cell model.

First, we see that the curve of reference parameters without dielectric is clearly a scenario less interesting than the 3 with Al_2O_3. Moreover, one should also notice the effect of having an increase of the Young's modulus. Indeed, the curve for reference parameters and AlN is clearly shifted to the right compared to the one simulated with Al_2O_3. But the most interesting is to compare the second curve with the ones obtained with the first candidate. Let's first focus on the similar devices, without dielectric below the piezoelectric. Compared to the reference curve, the candidate presents resonant and anti-resonance frequencies that are lower by approximately 150 and 90 MHz respectively. This confirms the increase of the coupling, as expected, but we do not know if it is associated with the apparition of perturbations (simulations using the other models would be needed to answer this question). For the model with dielectric below the piezoelectric material, it is worth noting that the anti-resonance frequency is almost constant, while the resonant frequency is reduced by approximately 85 MHz. Again, the coupling will be improved.

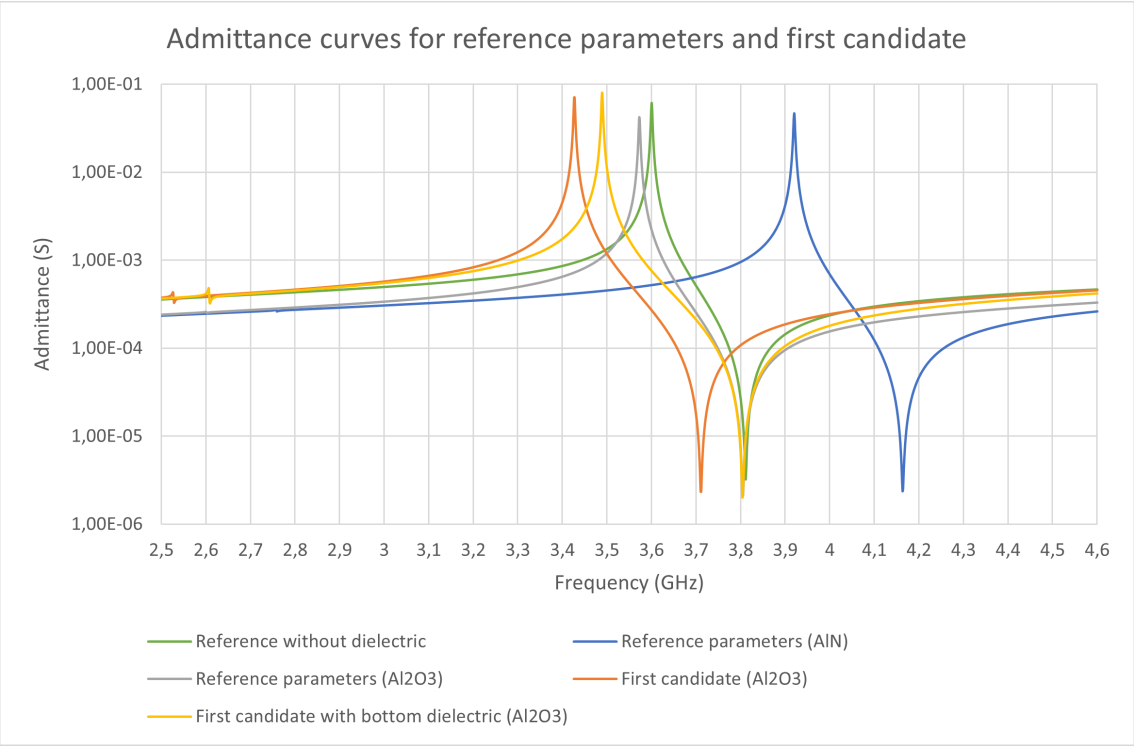

Figure 48: Comparison of the admittance curves for reference parameters (with $\lambda = 1\ \mu m$) and first candidate (2D unit cell)

However, it is important to notice a last fact before considering that these parameters are optimal. Indeed, recall that figure 34 has shown an inversion of performance between $\lambda = 1\ \mu m$ and $\lambda = 1.6\ \mu m$ when a certain value of $duty\ factor$ is attained. This result was then considered almost anecdotal, because the other parameters were all associated to a better behaviour for $\lambda = 1\ \mu m$. Nevertheless, the dielectric used was AlN and, we have seen that using Al_2O_3 and adding a dielectric layer below the piezoelectric induce both surprising behaviours of the resonator for $\lambda = 1\ \mu m$. For these reasons, it is important to simulate the behaviour of the new device using $\lambda = 1.6\ \mu m$, to verify if the combined effect of this change will not modify the trend observed with AlN.

Figure 49 shows the impact of the $\frac{t_{metal}}{\lambda}$ ratio on the coupling for this new configuration. The resulting couplings are very high compared to previous results (see table 3 for more details), and in particular, they are higher than the values obtained for $\lambda = 1\ \mu m$, proving that the results previously demonstrated with AlN cannot always be transposed to Al_2O_3.

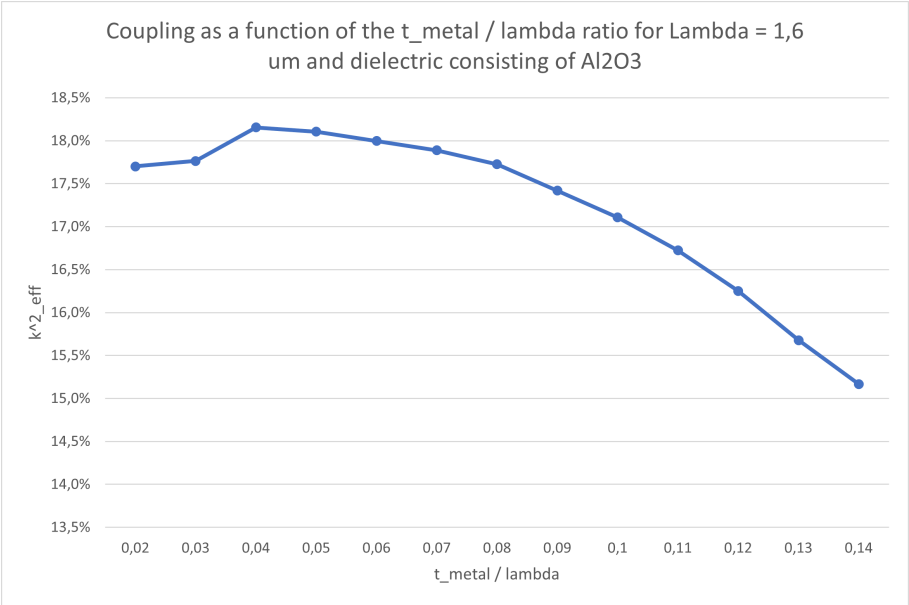

Figure 49: Coupling for different $\frac{t_{metal}}{\lambda}$ ratios when $t_{dielectric} = 20\ nm$ (Al_2O_3) and $\lambda = 1.6\ \mu m$

By performing other simulations on the device, it is even possible to improve again the coupling using $\lambda = 1.6\ \mu m$, but this step is not presented here because it has little added value (the result is however given in table 3 where all final results are summarized).

Figure 50 shows also the impact of the $\frac{t_{metal}}{\lambda}$ ratio, but for $\lambda = 3.2$ and $1\ \mu m$. Again, the step consisting of finding the adequate value for $t_{dielectric}$ is not given.

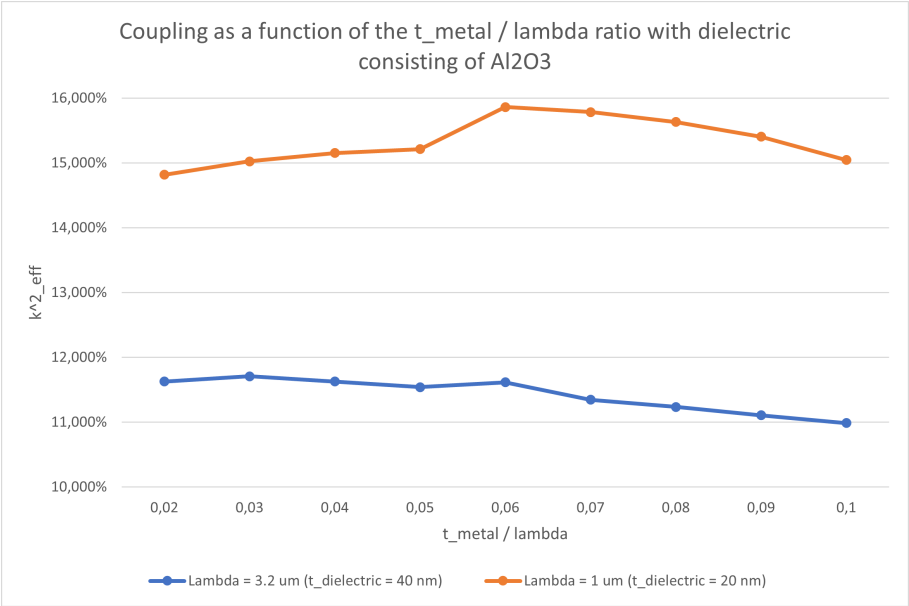

Figure 50: Coupling for different $\frac{t_{metal}}{\lambda}$ ratios when the dielectric is Al_2O_3

Table 3 summarizes some of the values obtained for k^2_{eff}, in order to better understand the impact of a change in parameter and the improvement obtained with optimal parameters. In particular, it contains the couplings obtained without dielectric (at the beginning) and 3 combinations of parameters for each λ (at the end): the bests for AlN and Al_2O_3 without dielectric below the device, and the best with dielectric below for Al_2O_3 (because it gives the highest couplings).

λ	t_{metal}	Dielectric (top)	Dielectric (bottom)	$t_{dielectric}$	$Duty\ factor$	k^2_{eff}
3.2 μm	100 nm	X	X	X	0.3	8.27%
1.6 μm	100 nm	X	X	X	0.3	10.61%
1 μm	100 nm	X	X	X	0.3	10.77%
3.2 μm	100 nm	AlN	X	50 nm	0.3	8.31%
1.6 μm	100 nm	AlN	X	50 nm	0.3	11.28%
1 μm	100 nm	AlN	X	50 nm	0.3	11.33%
3.2 μm	100 nm	Al_2O_3	X	50 nm	0.3	9.66%
1.6 μm	100 nm	Al_2O_3	X	50 nm	0.3	12.78%
1 μm	100 nm	Al_2O_3	X	50 nm	0.3	11.87%
3.2 μm	150 nm	AlN	X	50 nm	0.3	8.21%
3.2 μm	200 nm	AlN	X	50 nm	0.3	8.35%
1 μm	100 nm	AlN	X	20 nm	0.3	12.21%
1 μm	100 nm	AlN	X	40 nm	0.3	11.68%
1 μm	100 nm	AlN	X	60 nm	0.3	11.06%
1 μm	100 nm	AlN	X	80 nm	0.3	10.57%
1 μm	100 nm	AlN	X	50 nm	0.2	9.87%
1 μm	100 nm	AlN	X	50 nm	0.4	12.33%
1 μm	100 nm	AlN	X	50 nm	0.5	12.85%
1 μm	100 nm	AlN	X	50 nm	0.54	12.94%
1 μm	100 nm	AlN	X	50 nm	0.6	12.90%
1 μm	110 nm	AlN	X	20 nm	0.54	14.19%
1 μm	60 nm	Al_2O_3	X	20 nm	0.54	15.86%
1 μm	**60 nm**	**Al_2O_3**	✓	**20 nm**	**0.54**	**17.73%**
1.6 μm	128 nm	AlN	X	20 nm	0.54	14.35%
1.6 μm	64 nm	Al_2O_3	X	30 nm	0.54	15.40%
1.6 μm	**64 nm**	**Al_2O_3**	✓	**40 nm**	**0.54**	**18.66%**
3.2 μm	200 nm	AlN	X	20 nm	0.54	10.98%
3.2 μm	100 nm	Al_2O_3	X	40 nm	0.54	11.70%
3.2 μm	**100 nm**	**Al_2O_3**	✓	**40 nm**	**0.54**	**14.71%**

Table 3: Comparison of the couplings obtained for different configurations (2D unit cell)

4 Conclusion and discussion

Throughout this project, many simulations have been performed in order to better understand the behaviour of SH0 resonators, particularly in water, which was used to approximate a cellular environment. Compared to previous projects that have been conducted in the lab, 3 main differences appear. First, only the coupling was supposed to be optimized, and not the quality factor. Second, this work focuses on the optimization of the active region of the resonator only. Finally, a layer of dielectric is applied above the resonator, which strongly influences its behaviour.

But, before analyzing the device in an environment composed of water, it was important to perform simulations in air, to better understand the influence of the parameters and observe if it is constant from one environment to another. Many parameters have therefore been modified : the metal thickness, dielectric thickness, λ, duty factor, number of electrodes, and even the material of the dielectric used. And, if general behaviours are observed in air, we have seen that it is much more complicated in water, particularly when λ is reduced, because it is associated with high nonlinearities. For example, while an increase of $t_{dielectric}$ was systematically associated with a decrease of the coupling in air, in water, a small layer is useful to "protect" the device from the deleterious environment. Similarly, the value of duty factor used at the beginning of the project (0.3) originates from previous studies conducted in the laboratory, showing that it gives the best coupling in air. But, in water, increasing its value towards a certain threshold (0.54) allows to reduce the losses in water, and therefore increases the coupling. Above this value however, the electrodes become too close, which generates a drop of performance.

It has also been shown that, when results are observed with one dielectric, they sometimes differ with another. Therefore, when considering a change of dielectric, it is always important to perform new simulations, because it could generate strong differences with what is observed in this work. Concerning the dielectric, the positive impact of adding a layer below the piezoelectric has also been demonstrated. Indeed, it allows to increase the coupling by $2-3$ pp, which is very substantial when it is evaluated around 12-15%. However, given the complexity of adding this layer of dielectric, it will probably not be implemented in a real device.

Some results are nevertheless surprising. For example, while in air, larger λs produce higher values of coupling, in water, it is more complicated, with the largest evaluated value of λ producing the lowest coupling while the intermediate value produces the best coupling. The strong and deleterious influence of water on the performance of the resonator and the expected effect of λ on the coupling (larger values associated with larger couplings) probably compensate each other, leading to this unexpected observation.

This work has also shown the very good concordance between the 3 models used. Indeed, simulations in 2D unit cell and 2D complete have always given very close results, as well as admittance curves that were almost superimposed (if we do not consider the upward shift). The 3D unit cell model, however, is more complicated, because it allows spurious modes to appear between the resonant and anti-resonance frequencies. Nevertheless, despite their presence, couplings were still coherent with values obtained in 2D. Therefore, future studies could be performed using the 2D unit cell model to reduce the computational time (unless the parameters studied do not appear in this model).

In the end, it was possible to optimize the parameters for all λs, leading to higher values of couplings than the initial ones. For $\lambda = 3.2, 1.6$ and 1 μm, we have thus observed an increase of the coupling of respectively $77.87, 75.87$ and 64.62% respectively. However, it doesn't mean that we cannot do better and that the results should be taken as they are. Indeed, first, the combination of parameters should be tested in real conditions, to verify if they work, and if the values of coupling obtained above are coherent. Second, we have considered water only in the electrostatic domain, not in the mechanical one. Therefore, the coupling is probably slightly overestimated. Third, even if AlN is a piezoelectric material, we have only considered its influence as a dielectric and therefore, it could possibly induce other effects that were not taken into account (for example the spurious modes could be modified). Fourth, there are presumably other ways that allow to improve even more the coupling, either by using different configurations of devices (for example by trying to restrain the quantity of water in contact with the device to limit the losses), or because the values given in table 3 could still be optimized.

In further studies, it would be interesting to investigate other parameters, for example the thickness of the piezoelectric, but also the influence of the pistons when performing simulations in 3D models. Indeed, recall that they are used to reduce the spurious modes. However, in this work, they are not present in the 3D unit cell model and therefore, we do not know if they play an important role (we know from previous studies that their impact is small in air, but in water, it still needs to be demonstrated). Another interesting subject would be to simulate the behaviour of YBAR devices (BAR = Bulk Acoustic Resonator): contrarily to what we have seen in this project, these devices operate thanks to a vertical electrical field. IDT are placed on the surface, while a floating electrode is located below the piezoelectric. This configuration could lead to very interesting values of couplings because, thanks to the vertical electrical field, losses through the environment are strongly reduced.

Finally, I would like to thank Professor Villanueva and Florian Hartmann for their support and their availability throughout this semester project.

References

[1] Vincent Thommen. FEM modelling of LAMB wave Resonators, 2020.

[2] Julien Despreaux. FEM modelling of LAMB wave Resonators, 2020.

[3] Clelia Egger. FEM modelling of LAMB wave Resonators, 2021.

[4] Muhammad Faizan. Development of Lamb wave resonators in thin film X-cut lithium niobate, 2021.

[5] Ruochen Lu, Ming-Huang Li, Yansong Yang, Tomás Manzaneque, and Songbin Gong. Accurate Extraction of Large Electromechnical Coupling in Piezoelectric MEMS Resonators. *Journal of microelectrimechanical systems*, 28(2), 2019.

[6] Zhe Chen, Jian Zhou, Hao Tang, Yi Liu, Yiping Shen, Xiaobo Yin, Jiangpo Zheng, Hongshuai Zhang, Jianhui Wu, Xianglong Shi, Yiqin Chen, Yongqing Fu, and Huigao Duan. Ultrahigh-frequency surface acoustic wave sensors with giant mass-loading effects on electrodes. *ACS Sensors*, 5(6):1657–1664, 2020.

[7] Elmeri Österlund, Jere Kinnunen, Ville Rontu, Altti Torkkeli, and Mervi Paulasto-Kröckel. Mechanical properties and reliability of aluminum nitride thin films. *Journal of Alloys and Compounds*, 772:306–313, 2019.

[8] Marie K. Tripp, Christoph Stampfer, David C. Miller, Thomas Helbling, Cari F. Herrmann, Christofer Hierold, Ken Gall, Steven M. George, and Victor M. Bright. The mechanical properties of atomic layer deposited alumina for use in micro- and nano-electromechanical systems. *Sensors and Actuators A: Physical*, 130-131:419–429, 2006. Selected Papers from TRANSDUCERS '05.

[9] Joab R. Winkler and J. Brian Davies. Elimination of Spurious Modes in Finite Element Analysis. *Journal of computational physics*, 56, 1984.

[10] M. Solal et al. A method to reduce losses in buried electrodes RF SAW resonators. *IEEE International Ultrasonics Symposium*, 2011.

5 Appendices

5.1 Comments about the devices

This section will be dedicated to comments about the devices simulated, but also the choice of certain parameters:

- In section 1.3, n has been defined as the number of pairs of electrodes in the 2D complete model. In reality, if n is equal to x, this means that there are x signal electrodes, $x-1$ grounded electrodes, and 2 half grounded electrodes at both edges, called reflectors. Therefore, there are as much area of signal and grounded electrodes, but 1 less entire grounded electrode.

- Throughout this work, the dielectric mainly used was AlN, even if Al_2O_3 gives generally better results. The reason behind the choice of the passivation materials originates from the fabrication process of the resonators. During the fabrication, the passivation (SiO_2, Al_2O_3 or AlN) is deposited via Atomic Layer Deposition or using sputtering. However, once the resonators are defined on the substrate, they need to be freed from the substrate in order to be later fed to the cells. To free the resonators, etching of the sacrificial layer underneath the structures has to be performed. The sacrificial layer used being an oxide layer, the technique developed to etch it and collect the devices is to create an atmosphere of vapor HF. During this last step, vapor HF will etch the sacrificial layer but also the SiO_2 and the Al_2O_3 if these are used as passivation. Therefore, we decided to use AlN which is not attacked by vapor HF in this last critical step. However, the goal would also be to develop a new way of liberating the resonators which wouldn't etch the passivation and that is why some simulations were done also with Al_2O_3.

5.2 Description of values used during the simulations

Name	Values simulated	Unit
λ	1, 1.6, 3.2	μm
n (2D complete)	7, 14, 35, 70	X
Duty factor	$0.2-0.6$ (steps of 0.02)	X
t_{metal}	100, 150, 200	nm
$t_{dielectric}$	$10-90$ (steps of 10)	nm
Aperture	30, 60, 90	μm
t_{env}	300, $\frac{\lambda}{2}$, 1600	nm
Dielectric material	AlN, Al_2O_3	X
$\frac{t_{metal}}{\lambda}$	$0.02-0.25$ (steps of 0.01)	X
Environment	Air, Water	X

Table 4: Values simulated

5.3 Observation of spurious modes

This section shows the mode shape of the spurious modes appearing with reference parameters (in air), without giving many comments on the figures. It seems that the more perturbations we observe before a spurious modes, the more peaks of displacement are present in the mode shape.

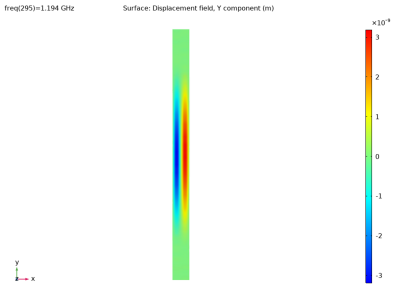

Figure 51: Displacement along transverse direction at resonant frequency (1.194 GHz)

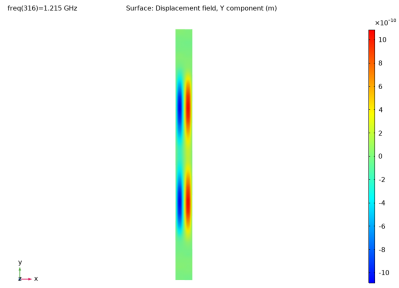

Figure 52: Displacement along transverse direction at resonance of first spurious mode

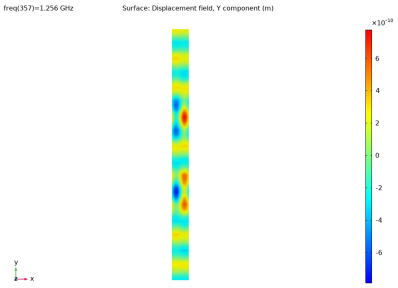

Figure 53: Displacement along transverse direction at resonance of second spurious mode

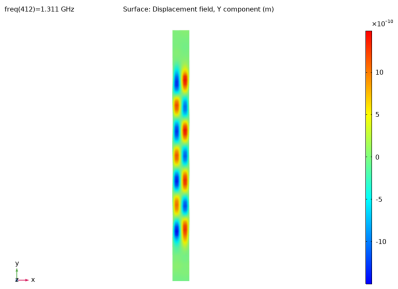

Figure 54: Displacement along transverse direction at resonance of third spurious mode

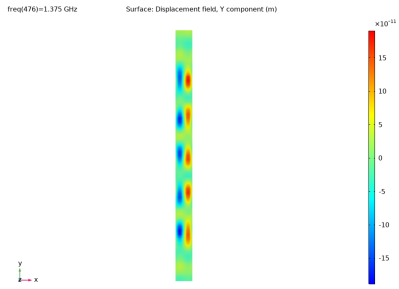

Figure 55: Displacement along transverse direction at resonance of fourth spurious mode

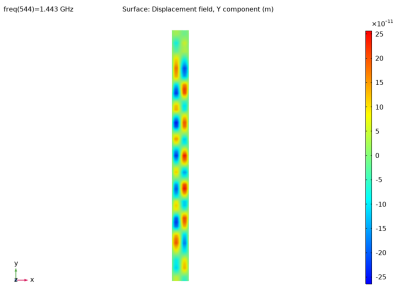

Figure 56: Displacement along transverse direction at resonance of fifth spurious mode